COUPLED STABILITY AND PERFORMANCE OF INTERACTION CONTROL THROUGH SERIES VISCOELASTIC ACTUATION

by Uğur Mengilli

Submitted to
the Graduate School of Engineering and Natural Sciences
in partial fulfillment of
the requirements for the degree of
Master of Science

Sabancı University July 2021

COUPLED STABILITY AND PERFORMANCE OF INTERACTION CONTROL THROUGH SERIES VISCOELASTIC ACTUATION

Approved	d by:		

Date of approval:

© Uğur Mengilli 2021 All Rights Reserved

COUPLED STABILITY AND PERFORMANCE OF INTERACTION CONTROL THROUGH SERIES VISCOELASTIC ACTUATION

Uğur Mengilli

Mechatronics Engineering M.Sc. Thesis, July 2021

Thesis Supervisor: Prof. Dr. Volkan Patoğlu

Keywords: Interaction control, physical human-robot interaction (pHRI), coupled stability, series elastic actuation (SEA), series viscoelastic actuation (SVA)

Abstract

Series Elastic Actuation (SEA) is a widely-used approach for interaction control as it enables high fidelity and robust force control, improving the safety of physical human-robot interaction (pHRI). Safety is an imperative design criterion for pHRI that limits the interaction performance since there exists a fundamental trade-off between stability robustness and rendering performance. The safety of interaction necessitates the closed-loop stability of a pHRI system when coupled to a wide range of unknown operators and environments. The frequency-domain passivity framework provides powerful analysis tools to study the coupled stability of linear time-invariant systems. In the literature, coupled stability of one-port models of SEA has been studied for various controllers while rendering basic environments, and the necessary and sufficient conditions for such passive terminations have been derived.

In this study, we advocate the addition of physical damping in parallel to the compliant element in SEA and provide sufficient conditions for the passivity of *series damped elastic actuation* (SDEA) under velocity-sourced impedance control (VSIC) while rendering virtual environments with null space, linear spring, or Kelvin-Voigt

(KV) models. We show the necessity of a physical dissipative element parallel to the series elastic component to render KV models and discuss the effect of an integral controller while rendering virtual environments modeled by a linear spring. Furthermore, we rigorously prove that SDEA can extend the range of impedances that can be passively rendered with SEA and improve the control performance of the system thanks to the physical damping in parallel to the compliant element.

We further extend our results to study the two-port passivity of SDEA under VSIC. We cascade a virtual coupler between the virtual environment and the controlled SDEA and study the coupled stability of SDEA under VSIC for all passive terminations. In particular, we introduce an analysis method based on Sturm's Theorem and provide the necessary and sufficient conditions for the two-port passivity of SDEA under VSIC within the frequency-domain passivity framework. We prove the necessity of additional dissipative elements in the physical filter and the virtual coupler for the two-port passivity of the system. Based on the newly established conditions, we derive non-conservative passivity bounds for the virtual coupler elements. We also show that these dissipative elements enable SDEA to display stiffer virtual environments than those can be passively rendered with an SEA. Finally, we validate our results through a set of physical experiments and systematic numerical simulations.

SERİ VİSKOELASTİK EYLEYİCİLER İÇİN GELİŞTİRİLEN ETKİLEŞİM KONTROLCÜLERİNİN KARARLILIĞI VE PERFORMANSI

Uğur Mengilli

Mekatronik Mühendisliği Yüksek Lisans Tezi, 2021

Tez Danışmanı: Prof. Dr. Volkan Patoğlu

Anahtar Kelimeler: Etkileşim kontrolü, fiziksel insan-robot etkileşimi, bağlaşık kararlılık, seri elastik eyleme, seri viskoelastik eyleme

Özetçe

Seri elastik eyleme (SEE), yüksek performanslı ve gürbüz kontrol sağladığı ve fiziksel insan-robot etkileşimini (fIRE) daha güvenli hale getirdiği için yaygın kullanılan bir etkileşim kontrolü yaklaşımıdır. Güvenlik fIRE için vazgeçilmez bir tasarım ölçütüdür; ancak gürbüz kararlılık ve başarım arasında temel bir ödünleşim olduğundan etkileşimin başarımını kısıtlar. Güvenli etkileşimin gerçekleşmesi için bir fIRE sisteminin, geniş bir yelpazede bilinmeyen çevresel etmenlerle etkileşimleri sırasında, kapalı çevriminin kararlı kalabilmesi—bağlaşık kararlı olması—gerekir. Doğrusal ve zamanla değişmeyen sistemlerin bağlaşık kararlılığını incelemek için frekans bölgesi pasifliği güçlü çözümleme araçları sağlar. Literatürde, SEE'nin tek kapılı ağ modellerinin bağlaşık kararlılığı çeşitli kontrolcüler altında temel sanal modeller için çalışılmış ve pasif dokunsal geri bildirim için gerekli ve yeterli koşullar bulunmuştur.

Bu çalışmada SEE'nin elastik elemanına paralel yerleştirilen fiziksel sönümleyicinin etkileri incelenmiştir. Empedans kontrolü altındaki seri viskoelastik eyleyici (SVE) ile sanal boş uzay, doğrusal yay ve Kelvin-Voigt (KV) modellerinin bağlaşık kararlı dokunsal geri bildirimi için sistemin tek kapılı pasiflik analizi yapılmış ve sistemin pasifliği için yeterli koşullar türetilmiştir. Fiziksel sönümleyicinin KV modelinin pasif dokunsal benzetimi için gerekli olduğu ve hız çevrimindeki integral kontrolün dokunsal benzetimde seçilebilecek yay sertliğine etkileri gösterilmiştir. Ek olarak, SVE'nin, SEE'nin pasif olarak gerçekleyebildiği empedans aralığını genişlettiği ve kontrolcü performansını arttırdığı ispatlanmıştır. Ayrıca, tek kapılı pasiflik sonuçları genişletilerek empedans kontrolü altındaki SVE'nin iki kapılı ağ modelinin pasifliği incelenmiştir. Sanal ortam ile kontrolcüler arasına sanal bir bağlantı modeli tanımlanarak sistemin iki kapılı pasifliğini sağlayacak gerekli ve yeterli koşullar bulunmuştur. Doğrusal ve zamanla değişmeyen sistemlerin pasifliğini frekans bölgesinde analitik olarak incelemek için Sturm teorisini temel alan bir yöntem sunulmuştur. SVE'nin iki kapılı pasifliği için fiziksel sönümleyiciye ek olarak sanal ara bağlantı modelinde de sönümleyici bir unsurun gerekliliği gösterilmiştir. Bu sönümleyiciler sayesinde pasif olarak gerçeklenebilecek sanal yayın sertliğinin arttırılabileceği kanıtlanmıştır. Son olarak, teorik sonuçlar sayısal benzetimler ve fiziksel deneylerle doğrulanmıştır.

Acknowledgements

I would like to express my sincere gratitude to my supervisor Professor Volkan Patoğlu for his support and fruitful discussions. His curiosity has been an excellent guide "into" countless scientific struggles, and his intelligence and experience have been a reassuring doorway out from them. I am grateful to him for helping me set my future directions. I also thank Assoc. Prof. Dr. Kemalettin Erbatur and Prof. Dr. Çağatay Başdoğan for their valuable feedback during my thesis defense and insightful suggestions for the completeness of this work. Special thanks to Assoc. Prof. Esra Erdem for supporting on a short training abroad and to Assoc. Prof. Güllü Kızıltaş Şendur, it was my pleasure to assist her at several undergraduate courses.

I thank the current and previous members of HMI Lab for sharing common joys and struggles: Ali KhalilianMotamed Bonab, Ali Yaşar, Ayhan Aktaş, Batuhan Toker, Bilal Çatkın, Burak Öztoprak, Cansu Öztürk, Celal Umut Kenanoğlu, Çağatay Irmak, Emre Cemal Gönen, Fatih Emre Tosun, Mahmut Beyaz, Umut Çalışkan and Zeynep Özge Orhan. I also want to thank Emre Yılmaz, Gökhan Alcan, İlker Sevgen, Mehmet Emin Mumcu, Mervenaz Şahin, Naida Fetic, Ömer Kemal Adak, and Serhat Aydın for our joyful conversations and their genuineness. Special thanks to Özge for informing me of Prof. Volkan Patoğlu and his search for graduate students, to Bilal, Ali, and Ali for their collaboration on our studies on AssistOn-Gait, again to Özge and Umut for our long work on SDEA, yet again to Ayhan, Gökhan, Kemal, Naida, and Umut for their reliable friendship and intellectual discussions.

It has been relieving and warming to feel the support of my friends and family wherever we go. I would like to thank METU Aikido Community, where I had so many everlasting connections that only a Ph.D. thesis would conceal the length of such an acknowledgment section if I started to write down even some of the names. But I know that we will meet somewhere around the world to compensate for that. I want to express my gratitude to Musab Çağrı Uğurlu, Payam Parvizi, Sinan Özgün Demir, and Utku Havuç for helping me out whenever I needed, both as a friend and

a colleague.

Lastly, I would like to thank my family and uncles Hasan and Cemal Mengilli for their endless support, especially during my education, which constitutes almost my whole life. I also thank my brother Okan for editing some of the figures in this thesis.

This study was partially supported by TÜBİTAK Grant 216M200.



Contents

A1	bstra	act					iv
Öz	zetçe						vi
A	cknov	wledgements					viii
Li	st of	Tables					xiv
Li	st of	Figures					xv
1	Intr	roduction					1
	1.1	Contributions					3
	1.2	Outline	•			•	5
2	Rela	ated Work					6
	2.1	Coupled Stability of SEA					7
	2.2	Physically Damped SEA					9
	2.3	Two-Port Analyses of Physically Damped SEA					11
3	Bac	ckground					13
	3.1	Network Modeling of Interaction Systems					13
		3.1.1 One-Port Networks					14
		3.1.2 Two-Port Networks					15
	3.2	Coupled Stability					15
		3.2.1 One-Port Passivity					16

		3.2.2	Two-Port Passivity	17
		3.2.3	Absolute Stability	18
	3.3	Perfor	mance Metrics of Haptic Systems	18
	3.4	Series	Elastic Actuation	19
		3.4.1	Uncontrolled S[D]EA Plant	20
		3.4.2	Velocity-Sourced Impedance Control of S[D]EA $\ \ldots \ \ldots$.	20
		3.4.3	Simplifying Assumptions	21
4	Stu	rm's T	Theorem for Testing Positive Realness	23
5	One	e-Port	Analysis of SDEA under VSIC	25
	5.1	One-P	Port Passivity Analysis	25
		5.1.1	Stability of SDEA under VSIC	26
		5.1.2	Passivity of Rendering the Kelvin-Voigt Model	28
		5.1.3	Special Cases: Passivity of Linear Spring and Null Space Ren-	
			dering	29
	5.2	Analy	sis of Rendering Performance	32
		5.2.1	Kelvin-Voigt Model	32
		5.2.2	Pure Linear Spring	33
		5.2.3	Null Impedance	33
	5.3	Discus	ssion and Conclusion	34
6	Two	o-Port	Analysis of SDEA under VSIC	36
	6.1	Two-F	Port Model of the System	36
		6.1.1	Coupled Stability of the Two-Port Network	37
		6.1.2	Insertion of the Virtual Coupler	39
	6.2	Two-F	Port Passivity Analysis	40
	6.3	Perfor	mance Analysis	48
		6.3.1	Transparency of the Two-Port Network	48
		6.3.2	Z-Width of the Two-Port Network	49
	6.4	Nume	rical Evaluations	50

		6.4.1	Passivity Analysis	51
		6.4.2	Performance Analysis	53
	6.5	Discus	sion	57
		6.5.1	The Necessity of Physical Damping	57
		6.5.2	The Necessity of Integral Gain of the Motion Controller	58
		6.5.3	The Effect of Virtual Coupler and System Dynamics on Two-	
			Port Passivity and Transparency	58
	6.6	Conclu	ısion	59
_	_		. 15. 1	
7	Exp	erime	ntal Evaluations	60
7	Exp 7.1		ntal Evaluations	
7	-			60
7	-	Experience 7.1.1	imental Setup	60 62
8	7.1	Experience 7.1.1 Verific	System Identification	60 62
8	7.1 7.2 Con	Experion Fig. 1.1.1 Verificately sectors of the se	System Identification	60 62 67

List of Tables

5.1	Nominal System Parameters	32
6.1	System parameters used for the numerical analysis	51
6.2	Maximum k_{22} values for the full-order (FO) system with different	
	feed-forward cancellation ratios compared to that of the FO system	
	analyzed under absolute stability	52
7.1	Estimated system parameters. All values are reflected to load-side	62
7.2	Estimated damper values. The distances are measured between the	
	two plates. Magnet tips are approximately 12.5 mm closer to the	
	aluminum plate	67

List of Figures

3.1	Network representations of a haptic rendering	14
3.2	Block diagram of SDEA under velocity-sourced impedance control (VSIC	!)
	coupled to a human operator	21
5.1	Performance comparison of SDEA and SEA under VSIC	33
5.2	Kelvin-Voigt model rendering of SDEA (solid lines) with the desired	
	stiffness and damping values (dashed lines)	34
6.1	Re-arranged block diagram of SDEA under VSIC that explicitly de-	
	picts the underlying two-port model	37
6.2	The network diagram and the corresponding block diagram of SDEA	
	under VSIC with a virtual coupler	38
6.3	Physical equivalent of the presented virtual coupler attached to a	
	virtual environment (VE is depicted as a spring)	40
6.4	Numerical evaluations of Condition $(c-ii)$ of Theorem 3.2	51
6.5	Performance of the two-port passive SDEA under VSIC	54
6.6	Kelvin-Voigt model rendering of the SDEA (solid lines) with the de-	
	sired stiffness and damping values (dashed lines)	56

7.1	Components of the experimental setup: Brushless DC motor (1),	
	$\operatorname{gearbox}{(2)},\operatorname{motor-side}\operatorname{capstan}\operatorname{drum}{(3)},\operatorname{load-side}\operatorname{capstan}\operatorname{drum}{(4)},$	
	cross-flexure leaf springs (5), linear encoder measuring the spring de-	
	flection (6), end-effector (7), aluminum plate of eddy-current damper (8),	
	permanent magnets and the holder plate (9), force/torque sensor for	
	parameter estimation (10), rotary encoder measuring the end-effector	
	angle for validations (11), motor driver (12), industrial PC (13)	61
7.2	The cumulative damping in the actuator and the gearbox depends	
	on the velocity. Among the curve models in MATLAB Curve Fitting	
	Toolbox, Weibull model fits the best (Adjusted $R^2=0.9112,\mathrm{RMSE}$	
	= 0.0012).	64
7.3	The cumulative inertia in the actuator and the gearbox is constant.	
	The negative values were considered outliers. A first-order polynomial	
	were used where the slope of the lines were always approximately zero	
	(Adjusted $R^2 = 1$, RMSE = 0.0092)	65
7.4	Validation of the torque estimation measuring the spring deflection. $$.	66
7.5	Estimation of the filter damping of SDEA. For this dataset, it is safer	
	to underestimate the damping value as $B = 0.08 \text{ N m s/rad}$	67

Chapter 1

Introduction

With robots rapidly being introduced in applications that require manipulation of objects [19,65] and interaction with unpredictable environments [24,51] and humans [8, 10, 21, 37, 45, 53, 56, 61, 62], safety has become an indispensable design requirement. Possessing inherent compliance and masking the inertia of the actuator from the interaction port, series elastic actuation (SEA) features favorable output impedance characteristics that are safe for physical interaction at all frequencies [32, 50, 51, 54, 55]. Due to these advantages, the coupled stability and performance characteristics of SEA have been widely studied under different control architectures [7, 47, 59, 60].

However, the control bandwidth of SEA within which it can achieve an acceptable force-rendering fidelity is reduced since large actuator forces/velocities are required to cancel out the compliant dynamics of SEA at high frequencies [50]. Moreover, the frequency-domain passivity analyses of SEA have established that the maximum virtual stiffness that can be rendered is bounded by the stiffness of the physical compliant element of SEA [59] while the Kelvin-Voigt (KV) model, i.e., parallel spring damper, cannot be passively rendered using causal controllers [7, 57]. In particular, KV models are commonly used to render virtual constraints by rigid haptic devices, but SEA has to sacrifice the stable rendering of this model for better interaction behavior.

Several studies have proposed using a physical damping parallel to the spring of SEA to improve its characteristics [20, 24, 36, 38, 39, 46, 47]. While these studies present advantages of SDEA over SEA, in terms of energy efficiency, reduction of the oscillations, and lack of need for D-control in joint-torque control, they have not addressed the coupled stability of interaction with SDEA during impedance rendering. Moreover, the two-port passivity of SDEA has not yet been investigated to enable stable interaction with all passive environments, unlike in rigid haptic devices [1,58] or bilateral teleoperation of robotic systems [29,40].

In this thesis, we first address the passive rendering of KV models using SDEA under velocity-sourced impedance control, a commonly used control structure for SEA [32,51,64]. Then, we seek to extend the range of impedance rendering to all possible passive terminations with unbounded magnitudes, ensuring the two-port passivity of the controlled SDEA.

1.1 Contributions

In this thesis, we present one-port and two-port frequency-domain passivity analyses of series damped elastic actuators (SDEA) under velocity-sourced impedance control (VSIC).

The contributions of this thesis can be listed as follows:

- We formulate an analytical method based on Sturm's theorem for analyzing the
 positiveness of polynomials encountered when assessing the positive realness of
 transfer functions. The proposed approach does not require the determination
 of roots of high degree polynomials but relies on systematic construction of
 tabular conditions and logical inference from these tables.
- We prove that a physical dissipative element *parallel* to the series elastic component is necessary to passively render KV models, regardless of the presence of a virtual coupler.
- We derive a set of *sufficient* conditions for SDEA under VSIC to passively render virtual environments modeled as parallel spring-dampers, as in the KV model, linear springs obeying Hooke's law, and the null impedance. We prove that SDEA can improve Z-width (the range of impedances that can be passively rendered) and the control performance of the system compared to SEA, thanks to the addition of the physical damping in parallel to the compliant element.
- We demonstrate that the integrator of the motion controller is *necessary* to render a virtual spring if there is an integrator in the force controller. Moreover, we also show that the bound on the maximum virtual stiffness can be increased significantly if both integrators are removed.
- We conduct two-port stability and transparency analyses of SEA/SDEA under VSIC. We rigorously prove the *necessity* of a virtual coupler with dissipation in addition to the physical damping for the two-port passivity of the system.

The additional dissipative elements enable the system to render virtual stiffness values higher than that can be rendered using a pure SEA. Our results extend earlier studies on coupled stability of SEA/SDEA by presenting the necessary and sufficient conditions for all passive terminations. We validate our theoretical results through numerical simulations and by reproducing one-port passivity results as special cases under appropriate terminations.

- Since the virtual coupler practically decreases the impedance transmitted to the operator, we propose simple formulae for selecting proper values of the virtual environment to compensate for the expected decrease.
- Our conditions assert that the integral action in the motion controller is *neces-sary* to insert a virtual coupler if there is an integrator in the force controller.
- We show that compensating for the disturbance due to the measured interaction force acting on SDEA may deteriorate the coupled stability of the system. Our results show that selection of an optimal cancellation ratio, which is strictly less than 1, can help maximize the virtual coupler stiffness while preserving the two-port passivity of the system.

1.2 Outline

The rest of the thesis is organized as follows:

Chapter 2 presents a comprehensive review of the related work on coupled stability of series elastic actuation and positions the contributions of this study concerning the state-of-the-art.

Chapter 3 overviews the concepts related to coupled stability and performance of interaction control. In particular, the frequency-domain passivity theorems for one-port and two-port networks are reviewed.

Chapter 4 presents a one-port passivity analysis of series damped elastic actuation under velocity-sourced impedance control.

Chapter 5 presents a two-port passivity analysis of series damped elastic actuation under velocity-sourced impedance control when augmented with a virtual coupled.

Chapter 6 details the experimental setup and provides experimental verification of one-port and two-port passivity results.

Chapter 7 concludes the thesis and provides a discussion of future research directions.

Technical details of certain proofs are provided in the Appendix.

Chapter 2

Related Work

The performance of SEA depends synergistically on its mechatronic design and controller [34,35]. The high-performance controller design for SEA to be used in pHRI is challenging since ensuring the safety of interactions is an imperative design requirement that constrains the design process. Safety of interaction requires coupled stability of the controlled SEA together with a human operator; however, the presence of a human operator in the control loop significantly complicates the stability analysis. In particular, a comprehensive model for human dynamics is not available, as human dynamics is highly nonlinear and time and configuration dependent. Contact interactions with the environment also pose similar challenges, since the impedance of the contact environment is, in general, uncertain.

The coupled stability analysis of robotic systems in the absence of human and environment models is commonly conducted using the frequency-domain passivity framework [15]. In this approach, even if the human operator behaves actively, coupled stability can still be concluded through the passivity analysis, as long as the human behavior is assumed to be non-malicious. Furthermore, non-animated environments are passive. Therefore, coupled stability of the overall system can be concluded, if the closed-loop SEA with its controller can be designed to be passive.

While the frequency-domain passivity paradigm provides robust stability for a

broad range of human and environment models, results derived from such analysis may be conservative. Less conservative paradigms, such as time-domain passivity [28, 52], complementary stability [4,6], bounded-impedance absolute stability [26, 42, 63], may be utilized to achieve better performance while still ensuring coupled stability of interaction. Although these techniques are highly valuable, they are limited in that they rely on numerical computations/optimizations; hence, they cannot provide closed-form analytical solutions and general insights. The frequency-domain passivity analyses are highly valuable as they provide a fundamental understanding of the underlying trade-offs governing the dynamics of the closed-loop system.

2.1 Coupled Stability of SEA

Coupled stability of SEA, modeled as an LTI system, has been investigated extensively using one-port passivity analysis, under several control architectures. Among these SEA control architectures, velocity-sourced impedance control (VSIC) [64] has been favored in the literature, due to its robustness, high performance, and ease of parameter tuning [10, 32, 49, 51, 59, 64].

Vallery et al. [60] have analyzed the passivity of VSIC architecture, without the motor damping in SEA model, for the case of zero reference torque. They have suggested conservative sufficient conditions for passivity based on the actuator inertia and a ratio between the controller gains. Later, they have extended this result for stiffness rendering with VSIC and proved that the passively renderable virtual stiffness is bounded by the stiffness of physical spring in the SEA [61].

Tagliamonte et al. [57] have shown that less conservative sufficient conditions for passivity can be derived for null impedance and pure stiffness rendering with VSIC architecture when the motor damping is included in the SEA model. In particular, it has been proven that the maximum achievable stiffness is not only related to the physical stiffness of the SEA, but also the physical damping in the system. They have

demonstrated that the Kelvin-Voigt model, which is a linear spring-damper pair in parallel, cannot be passively rendered using VSIC architecture. Later, they have also shown that the Maxwell model, which is a linear spring-damper pair in series, can be passively rendered using VSIC architecture [57], and derived *sufficient* conditions to characterize the range of environment parameters that preserve passivity.

Calanca et al. [7] have derived sufficient conditions for the passivity of SEA under several control architectures: basic impedance control, VSIC, collocated admittance control, and collocated impedance control. They have shown that the limitation on maximum achievable stiffness to render a pure stiffness, as derived in [61], also holds for these controllers. These theoretical analyses rely on the use of non-causal differentiator terms for the force controller and neglect the effect of motor damping in the system model. It is also stated in [7] that the KV model cannot be passively rendered with VSIC architecture and an impedance controller with ideal acceleration feedback has been suggested. Theoretically, ideal acceleration feedback can be used to cancel out the influence of load dynamics; however, noise and bandwidth restrictions of acceleration signals and potential overestimation of feed-forward signals resulting in feedback inversion are important practical challenges that have limited the adaptation of the acceleration-based control, since initially proposed in [50, 51].

Tosun and Patoglu [59] have derived the necessary and sufficient conditions for the passivity of VSIC architecture of SEA, relaxing the earlier established sufficiency bounds and extending the range of impedances that can be passively rendered. They have shown the necessity of integral gain of the motion controller to render pure stiffness. Furthermore, they have proven the necessity of a bound on the integral gains due to the inevitable physical damping in the system. This counter-intuitive bound indicates that the motor damping reduces the dynamic range of passively renderable impedances.

2.2 Physically Damped SEA

The main disadvantage of SEA is significantly decreased large force bandwidth caused by the increase of the sensor compliance under actuator saturation [50]. The selection of appropriate stiffness of the compliant element is essential in SEA designs, where a compromise solution needs to be reached between force control fidelity and large force bandwidth. Possible high-frequency oscillations of the endeffector, especially when the SEA is not in contact and the potential energy storage by the elastic element may pose as other challenges of SEA designs.

To address these issues, Newman has proposed a mechanical filter in the form of a parallel spring-damper [46]. He has also shown that the insertion of the damper can relax the passivity bounds of the system at frequencies greater than the natural frequency of the filter, and proposed a controller, called Natural Admittance Controller, guaranteeing the passivity of the system. Later, Dohring and Newman have further investigated the improvements of this filter on the system performance, especially at high frequencies [20].

The use of a physical damper instead of the series elastic element has been proposed in [14] to achieve similar improvements over SEA. It has been argued that series damper actuator (SDA) is favorable for force control, as it features an adequate level of force fidelity, low output impedance, and a large force range. Furthermore, it is shown through a theoretical analysis that SDA may increase the control bandwidth of the system, as it possesses a lower relative order in its transfer function compared to that of SEA.

Physically damped SEA concept has been studied in several other works in the literature [24, 33, 36, 38, 39, 47]. It is argued in [33] that impact forces may cause instability and chatter in SEA since the rapid accelerations cannot be achieved due to the rotor inertia and the motor torque limits. It has been shown through numerical simulations that *series damped elastic actuator* (SDEA) can increase the force control bandwidth.

To improve efficiency by avoiding continual energy dissipation due to constant

damping, SDEA with semi-active and variable damping have also been proposed. For instance, in [24], SDEA has been implemented for a legged robot using a magneto-rheological brake, where SDEA is controlled with a cascaded control architecture that has an inner force control loop and outer position control loop. Through physical experiments, it has been shown that adding parallel damping reduces oscillations and improves energy consumption.

In [39], the importance of damping to reduce oscillations has been highlighted, in the context of variable stiffness actuation. Within an admittance control scheme, it is stated that the introduction of damping acts as a phase lead after the resonance, resulting in improvements in the stability of the system. In [38], it has been shown that admittance controlled SDEA can achieve the same dynamic control performance of a conventional SEA, but with less effort, particularly for systems with a low natural frequency. It is also stated that although stability and control performance are enhanced, the level of actuator safety is compromised due to the increase of the transmitted force with the addition of damping.

In [23], numerical stability maps have been used to determine the viable range of stiffness and damping values for SDEA under a cascaded impedance controller with an inner torque loop acting on a velocity-compensated plant and load dynamics. Velocity compensation is implemented using a positive velocity feedback loop that aims to increase the bandwidth of the torque loop under passivity constraints.

In [36], conventional SEA and physical damped SEA structures have been compared from a control design perspective. The role of natural velocity feedback effect on force control performance is discussed, and the addition of physical damping to reduce the relative order of force dynamics is advocated. It is shown that through the addition of damping into SEA structure, derivative (D-control) terms become no longer necessary for the force control; therefore, acceleration feedback can be avoided. This study also suggests that robustness of SEA against impacts can be recovered by SDEA, if the transmitted damper force is mechanically limited, for instance, through a slip clutch.

While these studies present advantages of SDEA over SEA, in terms of energy efficiency, reduction of the oscillations and lack of need for D-control terms, they have not addressed the coupled stability of interaction with SDEA during impedance rendering. In [47], one-port passivity analysis for SDEA under basic impedance control has been presented. The control architecture utilized in this study is somewhat unconventional; in addition to the series damped elastic element, another force sensor is utilized after the end-effector inertia for measuring the human force, and this interaction force is fed back to the controller. In this study, Oblak and Matjačić [47] have shown that adequate level of mechanical damping in the compliant element is needed to ensure the passivity of pure stiffness rendering. Moreover, sufficient conditions for passivity and the lower bound on the required physical damping have been derived, in terms of the controller gains, motor-side damping, end-effector inertia, and motor-side inertia. While passivity of SEA/SDEA is independent of the end-effector inertia under conventional controllers, in this work, the use of the second force sensor after the end-effector introduces an additional bound on the proportional force controller gain that depends on the ratio of the actuator to the end-effector inertia.

2.3 Two-Port Analyses of Physically Damped SEA

In the literature, several works have conducted the coupled stability analysis of SEA/SDEA using a one-port passivity analysis, where the environments have a certain form. On the other hand, Tognetti [58] has studied a general haptic device with various virtual coupler forms considering two-port absolute stability. He has attempted to improve stability by inserting additional damping on the motor side. However, his analysis is numerical and does not provide general insights. In this study, we propose an analytical two-port passivity analysis of SDEA under VSIC with a virtual coupler. Two-port modeling provides an analysis framework that is advantageous in several ways:

- (i) Two-port passivity analysis ensures that the controller of SEA/SDEA can be designed independent of the environment to be rendered, as the coupled stability of the system can be ensured for any passive terminating environment. This may be especially useful if the environment characteristics are unknown to the device/controller designer, as commonly the case in haptic rendering [1], where the dynamics of the virtual environment rely on some external simulator.
- (ii) Using two-port analysis provides direct correspondence with the bilateral teleoperation literature and enables the passivity/transparency of the system to be analyzed analogously. For instance, the two-port representation of a haptic device provides an elegant way to observe the velocity/force transmission between the operator and the (virtual) environment.
- (iii) Two-port analyzes provide more general solutions, from which one-port results may be derived by properly terminating two-port element with an appropriate passive one-port [31].

Chapter 3

Background

This chapter reviews some fundamental concepts related to the modeling of interacting systems and the analytical tools commonly utilized in the literature and this study. There are several metrics defined to ensure the coupled stability and to evaluate the performance of interaction. We briefly provide some of the most acknowledged theories in the context of haptics and teleoperation.

3.1 Network Modeling of Interaction Systems

A network is a collection of interconnected elements and sources; however, a single lumped element (e.g., mass, spring, damper, etc.) can also be considered a network. Since networks may inherit some properties (e.g., [non]linearity, time-[in]variance, passivity, etc.) of the components comprising them, analyses of complex systems may be significantly simplified by abstracting these details away and dividing the problem into manageable parts.

The place where two networks exchange physical quantities or measured information is called a *port*. Regardless of the form of the interaction (e.g., mechanical, electrical, heat, digital signals, etc.), the systems exchanges their energies through the ports. Therefore, it is customary to model the ports using generalized power-conjugate quantities, called *effort* and *flow*. In electromechanical systems, it is

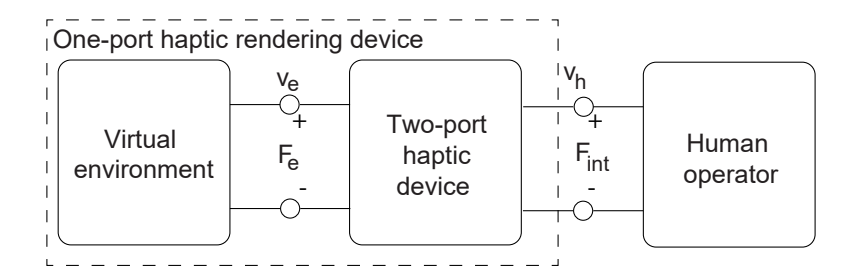


Figure 3.1: Network representations of a haptic rendering

common to represent voltages or forces as effort variables and currents or velocities as flow variables. Figure 3.1 shows a network that considers a physical interaction between a human operator and a haptic device and a digital interaction through the measured and calculated signals between a computer-generated virtual environment and the haptic device.

The following subsections describe general preliminary modeling details of oneport and two-port networks and discuss their advantages and disadvantages in analyzing interaction systems.

3.1.1 One-Port Networks

One-port networks have only one interaction point to exchange energy with its environment. The behavior of these systems can be expressed uniquely by the effort on and flow through the port. For the one-port haptic rendering device shown in Figure 3.1,

$$Z(s) = \frac{F_{\text{int}}}{v_h}, \quad Y(s) = \frac{1}{Z(s)} = \frac{v_h}{F_{\text{int}}}$$
(3.1)

where Z(s) and Y(s) are called the *driving point impedance* and the *driving point* admittance of the interaction port based on the choice of the independent variable (i.e., the input to the system), F_{int} represents the interaction force (the effort) between the operator and the end-effector of the device, and v_h denotes their mutual velocity (the flow).

3.1.2 Two-Port Networks

Two-port models have been adopted by the robotics to analyze the coupled stability [3] and performance [29] of haptic and bilateral teleoperation systems through the energy exchange analogy to the circuit theory. A two-port element can be represented by an *immittance matrix* that captures the relation between the effort (F_1, F_2) and the flow variables (v_1, v_2) .

Six distinct immittance matrices can be expressed based on the selection of the independent variables of the ports [31]. It is favorable to use the hybrid matrix (or h-matrix) when the input velocity and the output force are available via measurements [29]. By selecting these two as the independent variables, the following matrix relation describes the two-port element.

$$\begin{bmatrix} F_1 \\ v_2 \end{bmatrix} = \begin{bmatrix} h_{11} & h_{12} \\ h_{21} & h_{22} \end{bmatrix} \begin{bmatrix} v_1 \\ F_2 \end{bmatrix}. \tag{3.2}$$

In this form, h_{11} and h_{22} terms reveal important stability characteristics of the input and output ports. On the other hand, h_{12} (reverse force-transfer ratio) and h_{21} (forward velocity-transfer ratio) provide insights about the performance of the network.

3.2 Coupled Stability

The coupling of two stable systems does not necessarily result in a stable overall system since the dynamics of interaction is also important for stability. pHRI often demands robust stability while interacting with a wide range of environment and operator dynamics whose models are not available. Colgate and Hogan [15] have proposed the *frequency-domain passivity* to address the stability of interconnected systems.

Systems that do not produce energy are passive; hence, they are inherently stable. A useful property of passivity is that parallel and negative feedback interconnections of two passive systems also result in a passive system. This property can be used to ensure the stability of an interconnected system. Along these lines, *coupled stability* is defined as follows:

Definition 1 (Coupled Stability [16, 22]). A system has coupled stability property if:

- i) The system is stable when isolated.
- ii) The system remains stable when coupled to any passive environment that is also stable when isolated.

In frequency-domain passivity analysis, in general, the human operator is not assumed to be passive but is required to be non-malicious, i.e., does not aim to destabilize the system deliberately. For such interaction, human-applied inputs can be modeled to have a passive component and an intentionally applied active component that can be assumed to be independent of the system states. Given that state-independent active terms do not violate the coupled stability conclusions of the frequency-domain passivity, coupled stability can be concluded as if the human operator is passive when the state-independent active terms are neglected [15].

3.2.1 One-Port Passivity

Given a one-port, LTI, stable plant coupled to a passive environment, a necessary and sufficient condition for the coupled stability (see Definition 1) of the system is that the one-port is passive [16]. The driving point impedance Z(s) of a one-port LTI network is passive if and only if it is positive real [16,31].

Theorem 3.1 (Positive Realness [31]). An impedance function Z(s) is positive real if and only if:

- 1. Z(s) has no poles in the right half plane.
- 2. Any poles of Z(s) on the imaginary axis are simple with positive and real residues.

3. Re $[Z(j\omega)] \ge 0$ for all ω .

During haptic rendering, a human operator interacts with a virtual environment (VE) through the controlled device, as shown in Figure 3.1. In this figure, the operator and the VE can be considered as one-port elements, while the controlled device (excluding the VE dynamics) can be considered as a two-port network.

When the model of the VE to be rendered is known, then the two-port controlled device model can be terminated with this specific environment to form the one-port rendering model, as depicted by the dashed lines in Figure 3.1. Ensuring passivity of the driving point impedance Z(s) ensures coupled stability of interactions with a non-malicious human operator.

3.2.2 Two-Port Passivity

Two-port passivity analysis considers the controlled device, excluding the VE and human operator dynamics. Both the VE and human operator are assumed to be passive (with any active components being state independent). A sufficient condition of coupled stability of the overall system is the passivity of the two-port element. Note that two-port passivity is a conservative means of ensuring coupled stability. The necessary and sufficient conditions for the passivity of an LTI two-port element characterized by an immittance matrix H are given as follows:

Theorem 3.2 (Two-Port Passivity [31]). A linear time-invariant (LTI) two-port network is passive if and only if:

- (a) The h-parameters have no poles in the right half plane.
- (b) Any poles of the h-parameters on the imaginary axis are simple, and the residues are real and positive.
- (c) The h-parameters satisfy the following conditions for all ω .
 - (i) $Re(h_{11}) \ge 0$ and $Re(h_{22}) \ge 0$,

(ii)
$$\operatorname{Re}(h_{11})\operatorname{Re}(h_{22}) - \left|\frac{h_{12}^* + h_{21}}{2}\right|^2 \ge 0.$$

3.2.3 Absolute Stability

When a two-port network remains stable under all possible passive terminations, it is said to be absolutely or unconditionally stable [31]. Absolute stability is less conservative condition compared to two-port passivity. The necessary and sufficient conditions for absolute stability of an LTI two-port element characterized with an immittance matrix H can be expressed as follows:

Theorem 3.3 (Llewellyn's Absolute Stability [31]). A linear time-invariant (LTI) two-port network is absolutely stable if and only if:

- (a) The h-parameters have no poles in the right half plane.
- (b) Any poles of the h-parameters on the imaginary axis are simple, and the residues are real and positive.
- (c) h-parameters satisfy the following conditions for all ω .
 - (i) $Re(h_{11}) \geq 0$,
 - (ii) $2\operatorname{Re}(h_{11})\operatorname{Re}(h_{22}) \operatorname{Re}(h_{12}h_{21}) |h_{12}h_{21}| > 0.$

3.3 Performance Metrics of Haptic Systems

In addition to analysing coupled stability, two-port representation is also useful to study the performance of pHRI systems. A commonly used concept in haptic rendering and bilateral teleoperation literature is *transparency*, which quantifies the match between the mechanical impedance of the VE and that felt by the human operator, with the requirement of identical force/velocity responses. For a two-port system represented by its hybrid immittance matrix, ideal transparency is defined as [29, 30]:

$$\begin{bmatrix} F_1 \\ -v_2 \end{bmatrix} = \begin{bmatrix} 0 & 1 \\ -1 & 0 \end{bmatrix} \begin{bmatrix} v_1 \\ F_2 \end{bmatrix}. \tag{3.3}$$

If Z_e characterize the impedance of the VE, the impedance transmitted to the operator Z_{to} can be computed in terms of the parameters of the hybrid matrix as [30,31]

$$Z_{\text{to}} = \frac{h_{11} + \Delta_h Z_e}{1 + h_{22} Z_e},\tag{3.4}$$

where $\Delta_h = h_{11}h_{22} - h_{12}h_{21}$.

The difference between the minimum and the maximum achievable impedances of Z_{to} defines the range of passively renderable impedances, called Z_{width} [17]. In terms of hybrid matrix parameters, Z_{min} and Z_{width} can be computed as:

$$Z_{\min} = h_{11},$$
 (3.5)

$$Z_{\text{width}} = -\frac{h_{12}h_{21}}{h_{22}}. (3.6)$$

For the perfect transparency, Z_{\min} and Z_{width} go to zero and infinity, respectively.

3.4 Series Elastic Actuation

In this section, we present the dynamic modeling of SEA/SDEA under velocity-sourced impedance control (VSIC).

About the units and physical terms in this thesis: Although the physical entities in equations, figures, and tables represent rotational elements and corresponding units, linear counterparts of any entity may be used interchangeably throughout this thesis. Due to its more general usage, *forces* are preferred over *torques* without loss of generality.

3.4.1 Uncontrolled S[D]EA Plant

The dynamic model of the S[D]EA¹ consists of the reflected inertia J and viscous friction B of the actuator, which include effects of transmission and electrical dynamics, respectively. The actuator and the end-effector are connected by a spring with stiffness K_f that obeys the linear Hooke's law [and a viscous damper B_f , arranged in parallel]. Let the actuator and end-effector velocities be denoted by ω_m and ω_h , respectively. The forces applied by the human operator are modelled to have two distinct components: T_h representing the passive component and T_h^* denoting the intentionally applied active component that is assumed to be independent of the system states. The end-effector inertia is denoted by J_h . The interaction force $T_{\rm int}$ represents the sum of the forces induced on the linear spring [and the viscous damper arranged in parallel].

SDEA is similar to the SEA structure because both of them introduce a deliberate compliant element between the end-effector and the actuator. SEA estimates force by $T_{\rm int} = K_f \Delta \theta$ where $\Delta \theta$ is the measured deflection between the two bodies, and K_f is the spring constant. In SDEA, the estimated interaction force is $T_{\rm int} = K_f \Delta \theta + B_f \Delta \dot{\theta}$ where $\Delta \dot{\theta}$ is the rate of change of the deflection, and B_f denotes the damping coefficient of the physical filter. The rate of deflection is estimated by differentiating the output of a sensor directly measuring the deflection between the actuator and the end-effector/human.

3.4.2 Velocity-Sourced Impedance Control of S[D]EA

Figure 3.2 depicts the block diagram of SDEA under VSIC, where the physical interaction forces are denoted by thick lines. In particular, the cascaded controller comprises an inner velocity and an outer force control loops. While the inner loop renders the system into an *ideal motion source*, the outer loop generates references for the velocity controller such that the spring-damper deflections are at the desired

¹Due to the common components in a SEA and SDEA, we use brackets to denote any additional information belonging to SDEA.

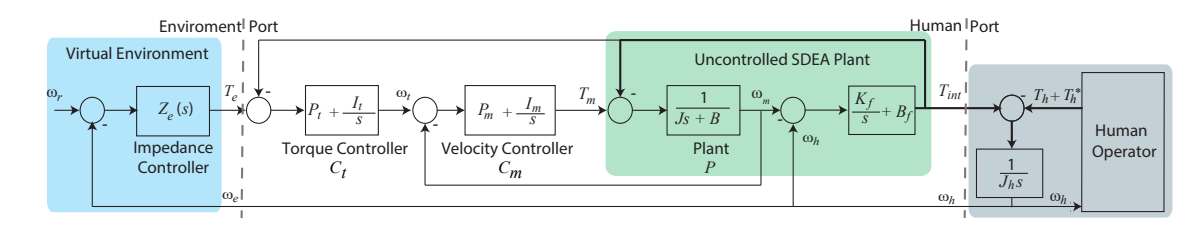


Figure 3.2: Block diagram of SDEA under velocity-sourced impedance control (VSIC) coupled to a human operator

level to match the reference force. To counteract steady-state errors, both velocity and force control loops employ PI controllers with gains denoted by P_m - I_m and P_t - I_t , respectively. The controllers do not include derivative action. Given that ideal differentiation is non-causal, filters that regulate the high-frequency phase response of the controller need to be considered for the soundness of the theoretical analysis. Besides, noise in force signals is known to significantly limit the practical use of derivative terms. Optionally, a feed-forward signal appends to the control signal to compensate for a portion (set by $1 - \alpha$ for $0 \le \alpha \le 1$) of the interaction force. The outermost loop implements an impedance controller to generate references to the force controller to display the desired impedance Z_e around the equilibrium v_r of the VE.

3.4.3 Simplifying Assumptions

Following simplifying assumptions are considered in theoretical discussions:

- Nonlinear effects, such as stiction, backlash, and motor saturation are neglected to develop a linear time-invariant (LTI) model. In the literature, it has been demonstrated that the cascaded force-velocity control scheme can effectively compensate for stiction and backlash [54,64]. If the motor is operated within its linear range, then the other nonlinear effects, like motor saturation, also vanish.
- The electrical dynamics of the system is approximated based on the commonly employed assumption that electrical time constant of the system is orders of

magnitude faster than the mechanical time constant.

- The motor velocity signal and the rate of change of deflections on the physical filter are available with a negligible delay. For motors furnished with high-resolution encoders, differentiation filters running at high sampling frequencies (commonly on hardware) can be employed to result in velocity estimations with minimum delays, within the bandwidth of interest.
- Human interactions are non-malicious and do not aim to destabilize the system deliberately. In particular, human applied inputs are modelled to have a passive component and an intentionally applied active component that is assumed to be independent of the system states [15]. This is a commonly employed assumption in the frequency-domain passivity analysis.
- For simplicity of analysis and without loss of generality, the VE is assumed to be grounded.

Chapter 4

Sturm's Theorem for Testing Positive Realness

Positive realness of an impedance function, as required in Condition (c) of Theorems 3.1–3.3 (passivity and absolute stability theorems), is commonly reduced to an equivalent problem of the positiveness of a polynomial by invoking the following Lemma.

Lemma 4.1. Let H(s) be any real-rational function such that

$$H(s) = \frac{N(s)}{D(s)}.$$

Positive realness of H(s) can be inferred from the positiveness of the following real polynomial.

$$\operatorname{Re}[(N(j\omega)D(-j\omega))] = \sum_{i=0}^{n} c_i \omega^i \ge 0, \quad \forall \omega, c_i \in \Re.$$

Proof. The proof is trivial and has been presented in several earlier works, including [59]. \Box

Analytical solutions to establish positiveness of a polynomial are well-established

for polynomials of up to degree three [13]. However, such analytical solutions becomes difficult for higher-order polynomials. Sturm, and later Vincent, have proposed simplified solutions to this problem by decomposing polynomials of degree n into the evaluation of lower degree sequences [2]. While Vincent's theorem is more efficient for numerical evaluations, we favor Sturm's theorem as it can also provide analytical bounds of positiveness of a polynomial. Below, we provide the definition of the Sturm sequence and Sturm's theorem [2].

Definition 2 (Sturm's Sequence or Chain [2]). Let f(x) = 0 be a polynomial equation of degree n, with rational coefficients and without multiple roots. The Sturm sequence is

$$S_{\text{seq}}(x) = \{ f(x), f'(x), r_1(x), r_2(x), \dots, r_k(x) \}, \tag{4.1}$$

where f'(x) is the first derivative of f(x) and the polynomials $r_i(x)$, $1 \le i \le k \le n-1$, are the *negatives* of the remainders obtained by applying the Euclidean greater common divisor algorithm on f(x) and f'(x), such that

$$f(x) = f'(x)q_1(x) - r_1(x)$$

$$f'(x) = r_1(x)q_2(x) - r_2(x)$$

$$\vdots$$

$$r_{k-2} = r_{k-1}(x)q_k(x) - r_k(x).$$

Theorem 4.1 (Sturm's Theorem of 1829 for real roots [2]). Let f(x) = 0 be a polynomial equation of degree n, with rational coefficients and without multiple roots. Then, the number ρ of its real roots in the open interval (a,b) satisfies the equality $\rho = \nu_a - \nu_b$, where ν_a , ν_b are the number of sign variations in the Sturm sequence $S_{\text{seq}}(a)$, $S_{\text{seq}}(b)$, respectively.

Utilizing Sturm's theorem, the positiveness of the polynomial f(x) can be found by setting the a and b to cover the entire frequency range, i.e., $\omega \in (-\infty, \infty)$.

Chapter 5

One-Port Analysis of SDEA under VSIC

5.1 One-Port Passivity Analysis

Given an LTI, stable plant coupled to a passive environment, the passivity of the oneport plant provides the necessary and sufficient conditions for the coupled stability of the overall system [16]. The frequency-domain passivity of a one-port LTI network is equivalent to the positive realness of the impedance Z(s) of the system at the interaction port [16]. The following analysis employs Theorem 3.1 to assess the positive realness of the one-port system.

This section derives a set of *sufficient conditions* for the frequency-domain passivity of SDEA under VSIC while rendering some commonly used virtual environment models: Kelvin-Voigt (KV), linear spring, and null space. Derivations are provided for rendering the KV model, and linear spring and null-space rendering are presented as special cases of this model when virtual damper and/or spring parameters are set to zero.

Following Theorem 3.1, the driving-point impedance at the human interaction port, shown in Figure 3.2, must be stable. For all virtual environments considered in this study, the stability requires the analysis of the same Routh array.

Lemma 5.1 imposes a stronger version of Condition (1) such that simple complex poles on the imaginary axis are not allowed. Furthermore, when a simple pole at the origin exists, it can be shown that its residue is non-negative for our analysis; thus, Condition (2) is always satisfied.

Therefore, the next subsection applies to all virtual environments considered, while the remaining subsections investigate Condition (3) of Theorem 3.1 for each environment.

5.1.1 Stability of SDEA under VSIC

The characteristic equation of the SDEA rendering the null-space has the form of a fourth-order polynomial with non-zero coefficients. The presence of a spring or a KV model in the virtual environment adds a simple pole at the origin, whose residue is non-negative. Since all cases correspond to the same Routh array, the following lemma will be utilized to ensure their stability.

Lemma 5.1 ([13,59]). Let $f_1(s) = a_4s^4 + a_3s^3 + a_2s^2 + a_1s + a_0$ or $f_2(s) = sf_1(s)$ for $a_i > 0$ be the characteristic equations of a fourth-order or fifth-order system, respectively. Then, $f_1(s)$ has no roots in the closed right half plane if and only if $a_1(a_2a_3 - a_1a_4) - a_0a_3^2 > 0$.

The driving-point impedance of SDEA under VSIC at the human port as shown in Figure 3.2 can be expressed as follows:

$$\frac{T_{\text{int}}}{-\omega_h} = \frac{B_f J s^5 + (K_f J + B_f (B + P_m) + b_4) s^4}{s (J s^4 + a_3 s^3 + a_2 s^2 + a_1 s + a_0)}, \quad (5.1)$$

where

$$b_{4} = B_{d}B_{f}P_{m}P_{t}$$

$$b_{3} = P_{m}P_{t}\left[K_{d}B_{f} + B_{d}\left(K_{f} + B_{f}\left(\mu + \nu\right)\right)\right]$$

$$b_{2} = B_{d}a_{1} + K_{d}P_{m}P_{t}\left(K_{f} + B_{f}\left(\mu + \nu\right)\right)$$

$$b_{1} = K_{d}a_{1} + B_{d}a_{0}$$

$$b_{0} = K_{d}a_{0}$$

$$a_{3} = B + P_{m} + B_{f}(1 + P_{m}P_{t})$$

$$a_{2} = I_{m} + K_{f}(1 + P_{m}P_{t}) + B_{f}P_{m}P_{t}(\mu + \nu)$$

$$a_{1} = K_{f}P_{m}P_{t}(\mu + \nu) + B_{f}I_{m}I_{t}$$

$$a_{0} = K_{f}I_{m}I_{t}$$

$$\mu = \frac{I_{m}}{P_{m}} \text{ and } \nu = \frac{I_{t}}{P_{t}}.$$

Given the system in Eqn. (5.1), the following stability condition can be derived using Lemma 5.1.

$$0 < a_3 \left[K_f^2 P_m P_t(\mu + \nu) (1 + P_m P_t) + I_m (K_f \kappa_1 + B_f I_m I_t) \right] + a_1 a_3 B_f P_m P_t(\mu + \nu) - a_1^2 J.$$
(5.2)

Remark 5.1. Note that the coefficients a_i of the characteristic equation are positive for positive proportional and non-negative integral gains. For passivity of null space and spring rendering, it is necessary that $\kappa_1 = I_m P_t - BI_t$ is positive, as discussed in Remarks 5.5 and 5.6. Hence, all terms except for the last one are positive in Eqn. (5.2). A high spring stiffness and high integral terms may destabilize the system, since a_3 is generally limited by the capacity of the actuator. Note that the addition of the physical damping to SEA increases the stability margin allowing higher controller gains.

5.1.2 Passivity of Rendering the Kelvin-Voigt Model

Haptic interactions with virtual constraints are commonly implemented with a KV model of the form $Z_e = K_d/s + B_d$ for penalty-based approaches. It has been established in the literature that SEA under VSIC cannot passively render KV models [57,59]. In this section, we prove the necessity of physical damping parallel to the compliant element, and present a set of sufficient conditions to passively render KV models with SDEA under VSIC.

Invoking Lemma 4.1 on Eqn. (5.1), it is necessary to ensure the positiveness of the polynomial below for all $\omega \in (-\infty, \infty)$.

$$(B_f J^2)\omega^{10} + c_8\omega^8 + c_6\omega^6 + c_4\omega^4 + (B_d K_f^2 I_m^2 I_t^2)\omega^2 \ge 0,$$
(5.3)

where

$$c_{8} = B_{f}(B_{f}\kappa_{3} + \kappa_{4} - K_{d}JP_{m}P_{t}) + B_{d}P_{m}P_{t}\left[B_{f}^{2}(1 + P_{m}P_{t}) + B_{f}\kappa_{2} - K_{f}J\right]$$

$$c_{6} = K_{f}P_{m}P_{t}\kappa_{2}\Delta K + K_{f}^{2}(B + P_{m}) + B_{f}^{2}I_{m}\kappa_{1} + B_{f}I_{m}^{2}$$

$$- K_{d}B_{f}\left[P_{m}P_{t}(B_{f} + B)(\mu + \nu) + I_{t}(P_{m}^{2} - JI_{m})\right]$$

$$+ B_{d}K_{f}\left[P_{m}P_{t}\{K_{f}(1 + P_{m}P_{t}) - B(\mu + \nu)\} - I_{t}(P_{m}^{2} - JI_{m})\right]$$

$$+ B_{d}B_{f}\left[B_{f}\{P_{m}^{2}P_{t}^{2}(\mu^{2} + \nu^{2}) - I_{m}I_{t}\} + I_{m}\kappa_{1}\right]$$

$$c_{4} = K_{f}\left[I_{m}\kappa_{1}\Delta K - K_{d}K_{f}P_{m}P_{t}(\mu + \nu)\right] - K_{d}B_{f}I_{m}^{2}I_{t}$$

$$+ B_{d}K_{f}\left[K_{f}\{P_{m}^{2}P_{t}^{2}(\mu^{2} + \nu^{2}) - I_{m}I_{t}\} - I_{m}^{2}I_{t}\right] + B_{d}B_{f}^{2}I_{m}^{2}I_{t}^{2}$$

$$(5.6)$$

with $\Delta K = K_f - K_d$ and

$$\kappa_1 = I_m P_t - B I_t,$$
 $\kappa_2 = (B + P_m) - J(\mu + \nu),$

$$\kappa_3 = (B + P_m) + P_m P_t \kappa_2,$$
 $\kappa_4 = (B + P_m)^2 - 2I_m J.$

A sufficient condition to satisfy Eqn. (5.3) is to ensure all coefficients in Eqn.s. (5.4)–(5.6) are non-negative. Then, these conditions together with the stability condition

in Eqn. (5.2) constitute a set of *sufficient* conditions for the passivity of SDEA under VSIC while rendering KV models.

Remark 5.2. For positive realness, it is necessary to ensure the positiveness of the highest and the lowest-order terms of any polynomial formed by utilizing Lemma 4.1. Since setting $B_f = 0$ makes Eqn. (5.4) negative, the introduction of a damping term in parallel to the physical compliant element is necessary to render KV models passively using VSIC.

Remark 5.3. The sufficient conditions given by Eqn.s. (5.4)–(5.6) result in three linear inequalities in terms of K_d and B_d . Increasing K_d negatively affects these conditions, while the effect of B_d depends on the selection of the system parameters. By solving these inequalities simultaneously, the most restrictive sufficient condition that ensures the passivity of the system can be obtained.

5.1.3 Special Cases: Passivity of Linear Spring and Null Space Rendering

Following the same procedure in the previous subsection, sufficient conditions for passively rendering pure spring and null-space models can be derived. These conditions are equivalent to the sufficient conditions for KV model rendering when B_d and/or K_d parameters are set to zero.

Linear Spring Rendering

For $B_d = 0$, Eqn. (5.3) is reduced to Eqn. (5.7).

$$(B_f J^2)\omega^{10} + c_8^s \omega^8 + c_6^s \omega^6 + c_4^s \omega^4 \ge 0, (5.7)$$

where

$$c_8^s = B_f(B_f \kappa_3 + \kappa_4 - K_d J P_m P_t) \tag{5.8}$$

$$c_{6}^{s} = K_{f}P_{m}P_{t}\kappa_{2}\Delta K + K_{f}^{2}(B + P_{m}) + B_{f}^{2}I_{m}\kappa_{1} + B_{f}I_{m}^{2}$$

$$-K_d B_f \left[P_m P_t (B_f + B)(\mu + \nu) + I_t (P_m^2 - J I_m) \right]$$
 (5.9)

$$c_4^s = K_f [I_m \kappa_1 \Delta K - K_d K_f P_m P_t(\mu + \nu)] - K_d B_f I_m^2 I_t.$$
 (5.10)

As in KV model case, for positive realness, it is sufficient to assure Eqn.s. (5.8)–(5.10) are non-negative. Then, these conditions together with Eqn. (5.2) comprise a set of sufficient conditions for passively rendering springs under VSIC.

Remark 5.4. Setting a positive integral gain I_m in the motion controller is necessary to passively render any virtual spring K_d if the integral gain I_t of the torque controller is non-zero. This result is in good agreement with and extends the stiffness rendering analysis of SEA under VSIC [59]. However, when both integral gains are zero, it is possible to render a virtual spring and increase the bound on it.

Remark 5.5. As discussed in Remark 5.2, Eqn. (5.10) is a necessary condition to satisfy Eqn. (5.7) and requires $\kappa_1 > 0$. Therefore, by setting $B_f = 0$, it is possible to derive necessary conditions for the passivity of SEA under VSIC while rendering a linear spring, as given in [59].

On the other hand, according to Eqn.s. (5.8)–(5.9), SDEA may allow significantly higher controller gains (i.e., I_m and I_t) than those possible with SEA, especially as the desired spring rate decreases, i.e., ΔK increases. Furthermore, the upper bound for pure stiffness rendering remains very close for SDEA and SEA when B_f is relatively low. These observations indicate that while SDEA can passively render a larger range of impedance than that of SEA, it can improve robustness by allowing higher controller gains. For instance, a higher I_m gain can significantly improve the tracking performance and disturbance rejection of the inner motion control loop, while a proper level of I_t may attenuate steady-state errors caused by constant torque disturbances.

Null Space Rendering

In this case, setting $B_d = 0$ and $K_d = 0$, Eqn. (5.3) becomes as follows.

$$(B_f J^2)\omega^{10} + c_8^n \omega^8 + c_6^n \omega^6 + c_4^n \omega^4 \ge 0, (5.11)$$

where

$$c_8^n = B_f(B_f \kappa_3 + \kappa_4) \tag{5.12}$$

$$c_6^n = K_f^2 \kappa_3 + B_f^2 I_m \kappa_1 + B_f I_m^2 \tag{5.13}$$

$$c_4^n = \kappa_1. \tag{5.14}$$

Sufficient conditions to render null-space can be claimed if Eqn. (5.2) holds and Eqn.s. (5.12)–(5.14) are non-negative.

Remark 5.6. While $\kappa_2 > 0$ is a sufficient condition for the stability of SEA under VSIC as presented in [57], this condition has been relaxed in [59] by providing the necessary condition as $\kappa_3 = (B + P_m) + P_m P_t \kappa_2 \ge 0$. Moreover, in [59], it has been proven that $\kappa_1 \ge 0$ is a necessary condition, which can also be concluded from Eqn. (5.14).

Remark 5.7. As noted in Remark 5.6, $\kappa_3 \geq 0$ and $\kappa_1 \geq 0$ are the necessary and sufficient conditions for SEA under VSIC to passively render the null space. Therefore, Eqn. (5.12) extends the SEA condition $\kappa_3 \geq 0$ if $\kappa_4 = (B + P_m)^2 - 2I_m J > 0$. Rearranging this term, one can derive

$$2\zeta_{\rm in}^2 = \frac{(B + P_m)^2}{2I_m J} > 1,$$

which suggests that if $\zeta_{in} > \sqrt{2}/2$, i.e., the inner control loop is overdamped, SDEA allows for higher controller gains while passively rendering null space. Since all terms in Eqn. (5.13) are positive, c_6^n is redundant for an underdamped inner loop. Although an underdamped system makes Eqn. (5.12) of SDEA stricter than the

necessary and sufficient conditions of SEA, a numerical analysis of necessity reveals that the sufficiency conditions can be significantly relaxed to provide a larger set of feasible controller gains compared to the necessary and sufficient conditions of SEA.

5.2 Analysis of Rendering Performance

While the coupled stability of pHRI systems constitutes an imperative design criterion, the performance of these systems are also significant for high-fidelity interactions. Although the analytical sufficient conditions derived in Section 5.1 are conservative, they provide a guidance in selecting a set of controller parameters that ensure the passivity. In this section, we enforce the passivity bounds through numerical evaluations and discuss the limits on the integral gains I_m and I_t for SDEA and SEA. Table 5.1 presents the nominal parameters employed for the numerical simulations.

5.2.1 Kelvin-Voigt Model

In this subsection, we study KV model rendering with $Z_e = K_d/s + B_d$. Figure 5.2 presents the KV model rendering performance of SDEA for different virtual environment parameters. The dashed lines in Figure 5.2 depict the desired impedances, while the solid lines indicate the output impedances rendered by SDEA under VSIC. From this figure, it can be observed that, unlike SEA, SDEA can passively render a

Param. Description Nominal Value Unit Stiffness of SDEA 362 N.m/rad K_f B_f Damping of SDEA 0.05 N.m.s/rad $kg.m^2$ JInertia of the actuator $0.640 \ 10^{-3}$ BDamping of the actuator 0.169N.m.s/rad P_m N.m.s/rad Proportional gain of the motion controller 0.28 I_m Integral gain of the motion controller 100 N.m/rad rad/N.m.s P_t Proportional gain of the torque controller 40 $rad/N.m.s^2$ 70 I_t Integral gain of the torque controller

Table 5.1: Nominal System Parameters

range of KV models thanks to the parallel physical damping.

5.2.2 Pure Linear Spring

In this subsection, we study the spring rendering with $Z_e = K_d/s$. Figure 5.1a compares the performance of SDEA with SEA under identical parameters.

The phase plots in Figure 5.1a with the same controller parameters show an improvement in the phase margin of SDEA due to the physical damping, which allows increased bounds on the controller gains. These plots also indicate that integral gains I_m and I_t can be significantly increased for SDEA without violating the passivity bounds. Higher I_m control gains improve the tracking performance and disturbance rejection of the inner motion control loop. Furthermore, the added physical damping smooths the resonance peaks displayed by SEA.

5.2.3 Null Impedance

In this subsection, we study null impedance rendering with $Z_e = 0$. Figure 5.1b compares the rendering performance of SDEA with SEA under identical system parameters. As in the spring rendering case, the physical damper allows significantly higher controller gains to be utilized by SDEA without violating passivity.

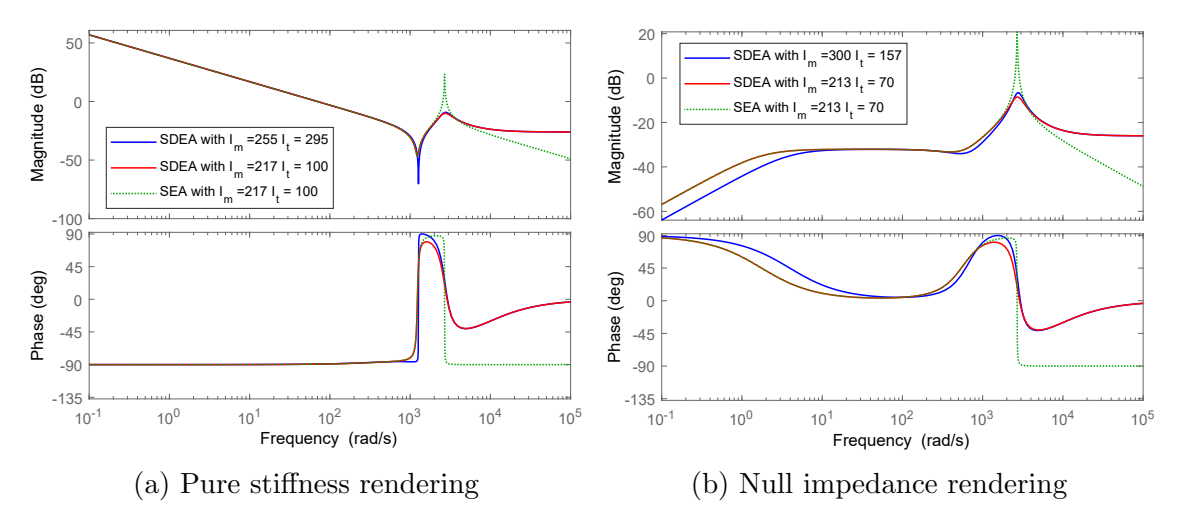


Figure 5.1: Performance comparison of SDEA and SEA under VSIC.

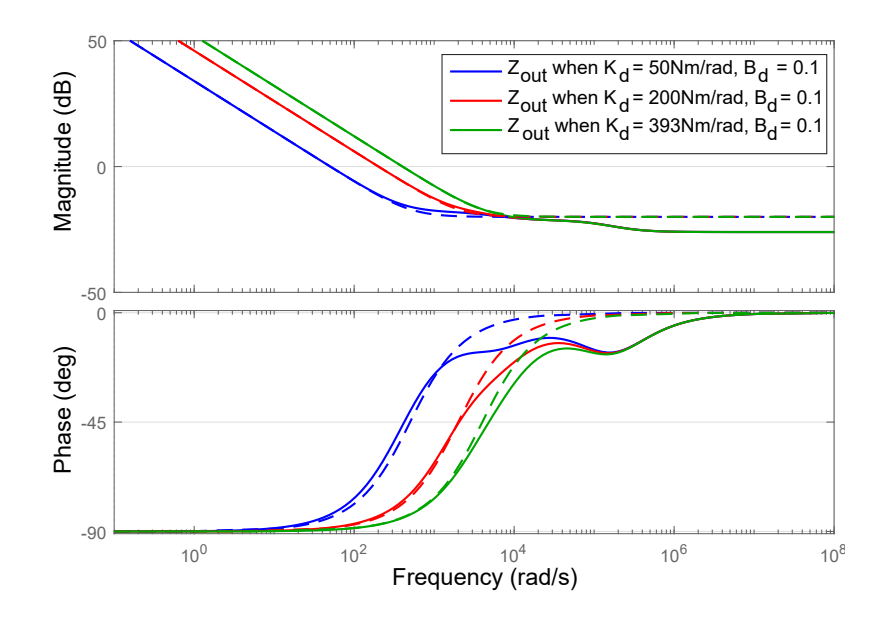


Figure 5.2: Kelvin-Voigt model rendering of SDEA (solid lines) with the desired stiffness and damping values (dashed lines).

Furthermore, the physical damping smooths the resonance peaks displayed by SEA.

5.3 Discussion and Conclusion

In this study, we have provided sufficient conditions for the passivity of SDEA under VSIC while rendering the most commonly utilized linear virtual environment models. We discussed the effects of the physical damping, plant parameters, and controller gains within these passivity limitations on the performance of haptic rendering.

It has been well-established in the literature that SEA under VSIC cannot passively render KV environments [57], while we have shown that the inclusion of physical damping allows SDEA to passively render KV models. Remark 5.2 proves the necessity of a physical damping term in parallel to the series elastic element for the passivity of the device when coupled to a KV model.

Remark 5.4 presents the necessity of the integral gain I_m of the motion controller (when $I_t > 0$) to ensure passivity of SDEA under VSIC to render a pure spring. This result is consistent with and generalizes a similar observation stated for the

passivity of SEA while rendering a pure spring [59].

We have also shown that the physical damping element B_f helps improve the control performance of the system by adding phase lead that can be allocated to increase controller gains, resulting in a more robust and responsive system.

While SDEA improves Z-width and control performance, it sacrifices ideal decoupling of the actuator dynamics under impacts and high-frequency disturbances at the interaction port. In particular, at the high-frequencies SDEA behaves like a damper, as can be observed in Figures 5.1a, 5.1b, and 5.2. Therefore, in terms of safety, low B_f levels may be preferred to limit the magnitude of impact forces. Alternatively, the robustness of SEA against impacts may be recovered by SDEA if the transmitted damping force is mechanically limited, for instance, through a slip clutch [36].

The frequency-domain passivity analyses are highly valuable as they provide a fundamental understanding of the underlying trade-offs governing the dynamics of the closed-loop system. For numerical implementations, less conservative paradigms, such as time-domain passivity [43], complementary stability [4,5], and mixed passivity and small-gain analyses [27], may be utilized to achieve better performance while still ensuring coupled stability of interaction.

Our ongoing works include investigating the effect of time delay and discretization on our passivity results.

Chapter 6

Two-Port Analysis of SDEA under VSIC

6.1 Two-Port Model of the System

In this section, we present the two-port dynamic modeling of SDEA under velocity-sourced impedance control (VSIC). To analyze the coupled stability of SDEA under VSIC, we model the closed-loop system as a two-port element that is terminated by a human operator at the input port and a passive (virtual) environment at the load port.

Selecting the input/output relationship to correspond to that of a hybrid immittance matrix, the two-port model can be expressed as:

$$\begin{bmatrix} F_{\text{int}} \\ v_e \end{bmatrix} = \begin{bmatrix} h_{11} & h_{12} \\ -1 & 0 \end{bmatrix} \begin{bmatrix} -v_h \\ F_e \end{bmatrix}, \tag{6.1}$$

where

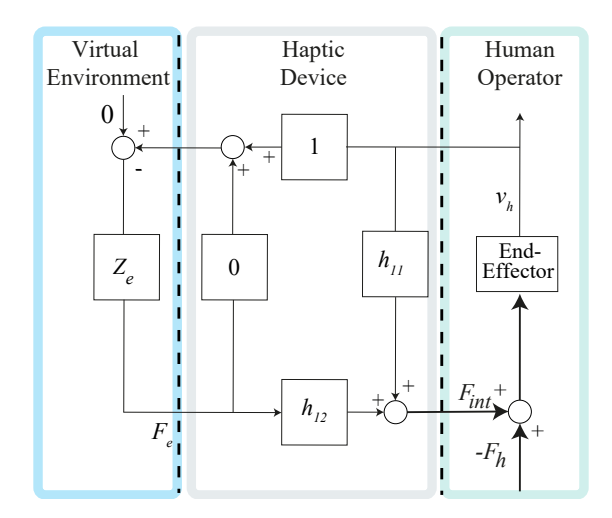


Figure 6.1: Re-arranged block diagram of SDEA under VSIC that explicitly depicts the underlying two-port model

$$h_{11} = \frac{(B_f s + K_f)(1 + C_m P)}{(1 + C_m P)s + P(B_f s + K_f)(\alpha + C_m C_f)}$$
$$h_{12} = \frac{C_f C_m P(B_f s + K_f)}{(1 + C_m P)s + P(B_f s + K_f)(\alpha + C_m C_f)}.$$

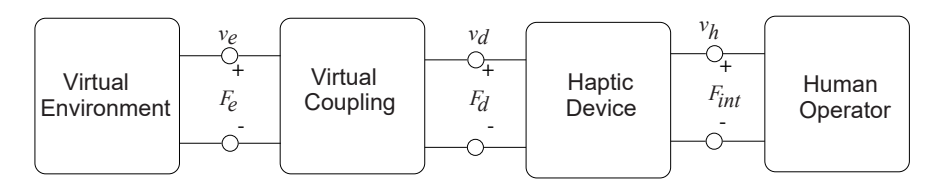
In this representation, P denotes the actuator dynamics, C_m and C_f denote generic motion and force controllers, respectively.

Figure 6.1 presents a re-arrangement of the block diagram in Figure 3.2, such that the underlying two-port model becomes explicit. For one to one correspondence with Figure 3.2, one can set $P = \frac{1}{Ms+B}$, $C_m = P_m + \frac{I_m}{s}$, and $C_f = P_f + \frac{I_f}{s}$.

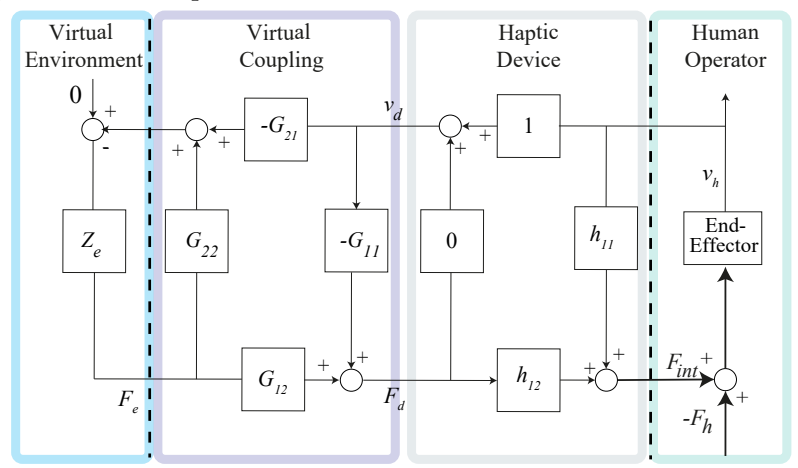
6.1.1 Coupled Stability of the Two-Port Network

The two-port model of controlled SDEA, as given in Eqn. (6.1), is neither two-port passive nor absolutely stable. Rigorous proofs of these facts are presented later in the manuscript, in Remark 6.1 and Lemma 6.5.

It is well-established in the literature that SEA under VSIC is not one-port passive while rendering pure springs with spring constants larger than the physical stiffness of SEA. Furthermore, it has also been shown that SEA under VSIC with



(a) Two-port network representation of SDEA under VSIC with a virtual coupler



(b) Block diagram in Figure 6.1 with a generic virtual coupler

Figure 6.2: The network diagram and the corresponding block diagram of SDEA under VSIC with a virtual coupler

integral controllers cannot passively render any VE having a KV model [57, 59]. Since two-port passive system can stably couple with any passive terminations, these results serve as counter-examples proving that the SEA under VSIC cannot be two-port passive.

SDEA under VSIC inherits a version of the physical stiffness upper-bound as in the SEA under VSIC while rendering pure stiffness. Furthermore, while SDEA under VSIC can passively render KV models thanks to the addition of damping element to its physical filter, passivity can be ensured for only a limited range of KV model parameters. Along these lines, SDEA under VSIC is also not two-port passive.

6.1.2 Insertion of the Virtual Coupler

Since the two-port model of SDEA under VSIC is not two-port passive, a virtual coupler (VC) is introduced before the VE, as suggested in the haptics literature [1, 18]. Figure 6.2 presents the network diagram and the corresponding block diagram of the system with a VC. The hybrid matrix for the SDEA with a generic virtual coupler reads as:

$$\begin{bmatrix} F_{\text{int}} \\ v_e \end{bmatrix} = \begin{bmatrix} h_{11} & h_{12} \\ G_{21} & G_{22} \end{bmatrix} \begin{bmatrix} -v_h \\ F_e \end{bmatrix}, \tag{6.2}$$

where

$$h_{11} = \frac{(B_f s + K_f)(1 + C_m P(1 + G_{11}C_f))}{(1 + C_m P)s + P(B_f s + K_f)(\alpha + C_m C_f)}$$
$$h_{12} = \frac{G_{12}C_f C_m P(B_f s + K_f)}{(1 + C_m P)s + P(B_f s + K_f)(\alpha + C_m C_f)}.$$

Transfer functions G_{ij} represent the two-port model of a generic VC. The transfer function G_{22} , virtual environment, and the device are in series, as shown in Figure 6.3. On the other hand, G_{11} is parallel to this structure, coupling the ground of the VE and the device. Transfer functions G_{12} and G_{21} represent the scaling factors between the forces and velocities, respectively.

Figure 6.3 presents a virtual coupler form that is commonly used in the literature [1, 18, 25]. In this model, a physical equivalent for G_{22} corresponds to a spring-damper pair (k_{22} and b_{22} , respectively) in parallel. Since haptic applications necessitate transferring the mechanical impedance of the VE transparently within stability regions, a natural selection for G_{22} would be a stiff coupling. At low frequencies, a stiff k_{22} achieves this goal while, at high frequencies, b_{22} compensates for the impedance drop of k_{22} . Later, in Section 6.2, we justify this selection in terms of the coupled stability of the system.

Formally, the mathematical model of this VC used in our analysis is as follows:

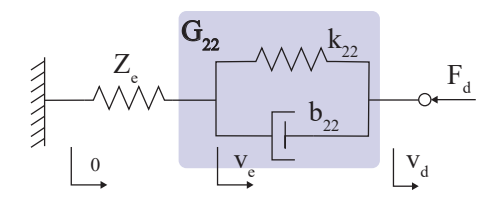


Figure 6.3: Physical equivalent of the presented virtual coupler attached to a virtual environment (VE is depicted as a spring)

$$G_{11} = 0, \quad G_{12} = -G_{21} = 1, \quad G_{22} = \frac{s}{b_{22}s + k_{22}}.$$
 (6.3)

Two-Port Passivity Analysis 6.2

In this section, we present the necessary and sufficient conditions for two-port passivity for SDEA under VSIC. To improve the readability of the section, we focus on the main results and present the proofs in the Appendix.

The hybrid matrix for the resulting two-port system can be expressed as:

$$\begin{bmatrix} F_{\text{int}} \\ v_e \end{bmatrix} = \begin{bmatrix} h_{11} & h_{12} \\ -1 & h_{22} \end{bmatrix} \begin{bmatrix} -v_h \\ F_e \end{bmatrix}, \tag{6.4}$$

where

$$h_{11} = \frac{B_f M s^4 + (B_f (B + P_m) + K_f M) s^3 + (B_f I_m + K_f (B + P_m)) s^2 + K_f I_m s}{a_4 s^4 + a_3 s^3 + a_2 s^2 + a_1 s + a_0}$$

$$(6.5)$$

$$h_{12} = \frac{B_f P_m P_f s^3 + P_m P_f (K_f + B_f (\mu + \nu)) s^2 + a_1 s + a_0}{a_4 s^4 + a_3 s^3 + a_2 s^2 + a_1 s + a_0}$$

$$h_{22} = \frac{s}{b_{22} s + k_{22}}$$
(6.6)

$$h_{22} = \frac{s}{b_{22}s + k_{22}} \tag{6.7}$$

with

$$a_{4} = M$$

$$a_{3} = B + P_{m} + B_{f}(\alpha + P_{m}P_{f})$$

$$a_{2} = I_{m} + K_{f}(\alpha + P_{m}P_{f}) + B_{f}P_{m}P_{f}(\mu + \nu)$$

$$a_{1} = B_{f}I_{m}I_{f} + K_{f}P_{m}P_{f}(\mu + \nu)$$

$$a_{0} = K_{f}I_{m}I_{f},$$

and

$$\mu = \frac{I_m}{P_m}, \quad \nu = \frac{I_f}{P_f}.$$

where h_{11} and h_{12} represent the system dynamics, and h_{22} contains the terms of VC.

Following lemmas are instrumental in the derivation of the necessary and sufficient conditions for two-port passivity for SDEA under VSIC.

Lemma 6.1 ([13,59]). Let $f(s) = a_4s^4 + a_3s^3 + a_2s^2 + a_1s + a_0$ for $a_i > 0$ be the characteristic equation of a fourth-order system. Then, f(s) has no roots in the open right half plane if and only if $a_1(a_2a_3 - a_1a_4) - a_0a_3^2 \ge 0$.

Proof. The proof has been presented in [59].

Lemma 6.2. Given a real-rational function

$$Z(s) = \frac{s(b_3s^3 + b_2s^2 + b_1s + b_0)}{a_4s^4 + a_3s^3 + a_2s^2 + a_1s + a_0},$$
(6.8)

where $a_i > 0$ and $b_i > 0$, Z(s) has a simple, conjugate pair of poles on the imaginary axis if and only if $a_1(a_2a_3 - a_1a_4) = a_0a_3^2$.

Proof. The proof is presented in Appendix A. \Box

Lemma 6.3. Consider the system in Eqn. (6.8), where $a_i > 0$, $b_i > 0$, and $a_1(a_2a_3 - a_1a_4) = a_0a_3^2$. The residues of the pair of poles on the imaginary axis are positive and real if and only if both of the following conditions hold.

(a)
$$a_1b_3 - a_3b_1 = (a_3b_0 - a_1b_2)a_3^2/(a_2a_3 - 2a_1a_4)$$

(b)
$$a_1b_3 - a_3b_1 < 0$$

Proof. The proof is presented in Appendix A.

Lemma 6.4. Let $p(x) = p_3x^3 + p_2x^2 + p_1x + p_0$ be any real polynomial. Then, $p(x) \ge 0$ for all $x \ge 0$ if and only if $p_3 \ge 0$ and $p_0 \ge 0$ and one of the following conditions holds:

(a)
$$p_1 \ge 0$$
 and $p_2 \ge -\sqrt{3p_1p_3}$

(b)
$$\sigma = p_2^2 - 3p_1p_3 > 0$$
 and $p_1p_2 - 9p_0p_3 < 0$ and $4p_2(p_1p_2 - 9p_0p_3) < 4p_1\sigma + 3p_3\frac{(p_1p_2 - 9p_0p_3)^2}{\sigma}$

Proof. Our proof is based on an application of Strum's theorem and is presented in Appendix A. An alternative geometric proof can be found in [13]. \Box

Utilizing Lemmas 6.1–6.4, Theorem 6.1 presents the necessary and sufficient conditions for two-port passivity for SDEA under VSIC.

Theorem 6.1. Consider SDEA under VSIC as in Eqn. (6.4), where K_f , M, B, P_m , P_f , k_{22} are taken as positive, while B_f , I_m , I_f , b_{22} are assumed to be non-negative. Then, this system is two-port passive if and only if Conditions (a)–(c) hold:

(a) The h-parameters have no poles in the right half plane

$$0 < a_3 \left[K_f^2 P_m P_f(\mu + \nu) (\alpha + P_m P_f) + I_m (K_f \kappa_1 + B_f I_m I_f) \right]$$

+ $a_1 a_3 B_f P_m P_f(\mu + \nu) - a_1^2 M$.

(b) If h_{11} , given in Eqn. (6.5), has a pair of poles on the imaginary axis, their residues are real and positive

(i)
$$0 < \beta = a_3 (K_f(B + P_m) + B_f I_m) - a_1(B_f M)$$
 and

(ii)
$$\beta(a_2a_3 - 2a_1a_4) = (a_3(K_fI_m) - a_1(B_f(B + P_m) + K_fM))a_3^2$$

- (c) The system parameters simultaneously satisfy the Conditions (i) and (ii):
 - (i) Condition (i1) or (i2) holds:

(i1)
$$0 \le r_1 = K_f^2 \kappa_3 + B_f I_m^2 + B_f^2 I_m \kappa_1$$

and
$$0 \le B_f ((B + P_m)^2 + B_f \kappa_3 - 2I_m M) + M \sqrt{3B_f r_1}$$
(i2) $0 < \rho_1 = B_f^2 ((B + P_m)^2 + B_f \kappa_3 - 2I_m M)^2 - 3B_f M^2 r_1$
and
$$0 > \rho_2 = r_1 B_f ((B + P_m)^2 + B_f \kappa_3 - 2I_m M) - 9B_f I_m M^2 K_f^2 \kappa_1$$
and
$$4\rho_2 B_f ((B + P_m)^2 + B_f \kappa_3 - 2I_m M) < 4r_1 \rho_1 + \frac{3B_f M^2 \rho_2^2}{\rho_1}$$

(ii) $k_{22}^2 \le 4b_{22}I_m(I_mP_f - BI_f) \left(\frac{K_f}{I_m + \alpha K_f}\right)^2$ and $0 < b_{22} \le 4B_f$ and Condition (ii1) or (ii2) holds:

(ii1)
$$0 \le t_1 = 4b_{22}r_1 + k_{22}^2\tau_2 - b_{22}^2(I_m + \alpha K_f)^2$$

and
$$0 \le 4b_{22}r_2 + b_{22}^2\tau_2 - k_{22}^2M^2 + M\sqrt{3b_{22}}$$
(ii2) $0 < \tau_3 = \left(4b_{22}r_2 + b_{22}^2\tau_2 - k_{22}^2M^2\right)^2 - 3M^2b_{22}\tau_1t_1$
and
$$0 > \tau_4 = t_1(4b_{22}r_2 + b_{22}^2\tau_2 - k_{22}^2M^2) - 9M^2b_{22}\tau_1t_0\kappa_1$$
and
$$4\tau_4(4b_{22}r_2 + b_{22}^2\tau_2 - k_{22}^2M^2) < 4t_1\tau_3 + \frac{3M^2b_{22}\tau_1\tau_4^2}{\tau_3}$$

where

$$\kappa_{1} = P_{f}I_{m} - BI_{f}$$

$$\kappa_{2} = B + P_{m} - M(\mu + \nu)$$

$$\kappa_{3} = \alpha(B + P_{m}) + P_{m}P_{f}\kappa_{2}$$

$$\tau_{1} = 4B_{f} - b_{22}$$

$$\tau_{2} = 2M(I_{m} + \alpha K_{f}) - (B + P_{m} + \alpha B_{f})^{2}$$

$$r_{2} = B_{f}((B + P_{m})^{2} + B_{f}\kappa_{3} - 2I_{m}M).$$

Proof. The proof is presented in Appendix A.

Remark 6.1. Two-port passivity necessitates SDEA, instead of SEA, and a damping element in the VC. In particular, according to Condition (c-ii) of Theorem 6.1, two-port passivity of SDEA under VSIC cannot be satisfied if $B_f = 0$ (i.e., there exist no physical damping as in the case of SEA) or $b_{22} = 0$ (i.e., VC does not incorporate a virtual damping). In this case, the highest-degree term of Eqn. (A.12) in the proof of Theorem 6.1 is reduced to

$$B_f = 0 \implies p_2 = -b_{22}^2 M^2 < 0,$$

violating two-port passivity. For the second case, the fifth-degree term drops leaving the highest term as

$$b_{22} = 0 \implies -k_{22}^2 M^2 < 0,$$

resulting in a similar violation.

Remark 6.2. Note that, we made use of Lemmas 4.1 and 6.4 in the derivation of the necessary and sufficient conditions of two-port passivity of the system. However, it is possible to obtain simpler, but only sufficient conditions to ensure passivity. In particular, if the system parameters are selected such that all coefficients of the polynomial given in Lemma 6.4 are positive, then the polynomial is positive for all

x. Then, Condition (c-i) of Theorem 6.1 is simplified to the following conditions.

$$0 \le r_0 : I_f \le \frac{I_m P_f}{B} \tag{6.9}$$

$$0 \le r_1 : 0 \le K_f^2 \kappa_3 + B_f I_m^2 + B_f^2 I_m \kappa_1 \tag{6.10}$$

$$0 \le r_2 : 0 \le B_f \kappa_3 + (B + P_m)^2 - 2I_m M. \tag{6.11}$$

Similar considerations simplify Condition (c-ii) to

$$0 \le t_0 : k_{22}^2 \le 4b_{22}I_m(I_mP_f - BI_f) \left(\frac{K_f}{I_m + \alpha K_f}\right)^2 \tag{6.12}$$

$$0 \le t_1 : 0 \le 4b_{22}r_1 + k_{22}^2\tau_2 - b_{22}^2(I_m + \alpha K_f)^2$$
(6.13)

$$0 \le t_2 : 0 \le 4b_{22}r_2 + b_{22}^2\tau_2 - k_{22}^2M^2 \tag{6.14}$$

$$0 \le t_3 : 0 < b_{22} \le 4B_f. \tag{6.15}$$

Then, sufficient conditions to ensure two-port passivity of the system given by Eqn. (6.4) can be stated as Conditions (a) and (b) of Theorem 6.1, and Eqn.s. (6.9) and (6.12). These equations form a set of explicit solutions of the virtual coupler elements (i.e., k_{22} and b_{22}), which is not available in Theorem 6.1.

Remark 6.3. The integral gain I_m of the motion controller is necessary so that the virtual coupler may have a non-zero stiffness k_{22} when the integral gain I_f of the force controller is non-zero. In particular, it follows from the first condition on k_{22} , Condition (c-ii) of Theorem 6.1, that if $I_m = 0$, then $k_{22} = 0$, leaving the virtual coupler with only a pure damping term b_{22} . Note that result is in good agreement with the one-port stiffness rendering analysis [59]. However, when both integral gains are zero, it is both possible to render a virtual spring and increase the bound on it.

Remark 6.4. In the analysis of the full-order system, $(1 - \alpha)$ modulates the state-dependent feed-forward action. In the first condition on k_{22} , in Condition (c-ii) of Theorem 6.1, if $\alpha = 0$, then k_{22}^{max} is increased. However, the other equations in Condition (c-ii) have inverse behavior with this result. Overall, completely canceling

the physical interaction force affects passivity adversely. Although it is hard to follow this result through the analytical expressions of Theorem 6.1, a numerical analysis reveals that there is an optimal value for α , as discussed in Section 6.4.1.

Remark 6.5. In general, Conditions (a)–(c-i) of Theorem 3.2 (excluding the conditions on h_{22}) are equivalent to those of Theorem 3.1, and lead to one-port passivity of a system described by h_{11} coupled to a null environment. Therefore, Conditions (a)–(c-i) presented in Theorem 6.1 generalize one-port passivity results presented in [59] for SEA under VSIC. In this equation, if $B_f = 0$, one can recover the necessary and sufficient conditions for passively rendering null impedance using the SEA under VSIC [59].

Remark 6.6. The necessary and sufficient conditions for two-port passivity presented in Theorem 6.1 can be relaxed by studying absolute stability¹ given in Theorem 3.3. Although the equations are hard to interpret, they are useful for numerical implementation. Numerical comparisons between two-port passivity and absolute stability are presented in Section 6.4.

Lemma 6.5. Consider SDEA under VSIC as in Eqn. (6.4), where K_f , M, B, P_m , P_f , k_{22} are taken as positive, while I_m , I_f are assumed to be non-negative. Let B_f be positive and let Conditions (a)–(c-i) of Theorem 6.1 are satisfied². Then the two-port model of the system can not be absolutely stable unless it incorporates a virtual coupler with some damping (i.e., $b_{22} > 0$).

Proof. Note that the Conditions (a)-(c-i) of Theorem 6.1 are equivalent to those of Theorem 3.3, since h_{22} is already passive. Following Theorem 3.3 for $b_{22} = 0$, Condition (c-ii) can be rewritten as follows.

$$-\operatorname{Re}(h_{12}h_{21}) - |h_{12}h_{21}| \ge 0.$$

 $^{^1{\}rm The~MATLAB}$ code is available in the public GitHub repository <code>https://github.com/ugurmengilli/SEA-2port-analysis.</code>

²Note that, Conditions (a)–(c-i) of two-port passivity (i.e., Theorem 3.2) and absolute stability (i.e., Theorem 3.3) are identical in this case.

We can further simplify this equation by setting $h_{21} = -1$:

$$\operatorname{Re}(h_{12}) \ge |h_{12}| = \sqrt{\operatorname{Re}(h_{12})^2 + \operatorname{Im}(h_{12})^2},$$

where the only possibility is that the system dynamics comprise pure damping. For any realistic design, it is not possible to manufacture the system without any mass or compliance in the system. Hence, in the virtual coupler, the damping element is required for satisfying absolute stability.

Lemma 6.6. Consider SDEA under VSIC as in Eqn. (6.4), where K_f , M, B, P_m , P_f , k_{22} are taken as positive, while I_m , I_f are assumed to be non-negative. Let b_{22} be positive and let Conditions (a)–(c-i) of Theorem 6.1 are already satisfied². Then, the two-port model of the system can not be absolutely stable unless it incorporates a physical coupler with a parallel a damping (i.e., $B_f > 0$).

Proof. Note that, the absence of B_f leads to SEA. Therefore, Conditions (a)–(c-i) of Theorem 6.1 correspond to the necessary and sufficient conditions for one-port passivity of SEA rendering null space (see Remark 6.5), as presented in [59]. When $B_f = 0$, Condition (c-i-2) of Theorem 6.1 becomes invalid and Condition (c-i-1) is reduced to

$$0 \le r_1 = (\alpha + P_f P_m)(B + P_m) - M P_m P_f(\mu + \nu). \tag{6.16}$$

Following Condition (c-ii) of Theorem 3.3 and Lemma 4.1 lead to a polynomial inequality of the form $0 \le x^2(p_5x^5 + p_4x^4 + p_3x^3 + p_2x^2 + p_1x + p_0)$. To ensure the positiveness of this high-degree polynomial, it is necessary that $p_5 \ge 0$ and $p_0 \ge 0$. However, we can deduce that $p_5 < 0$ under the condition given by inequality (6.16):

$$0 > p_5 = -b_{22}P_m P_f (((P_m + B) - M(\mu + \nu))^2 - 4r_1 M K_f,$$
 (6.17)

which concludes the proof.

To summarize, in this section the necessary and sufficiency conditions are derived for two-port passivity of SDEA under VSIC. The need for the damping element B_f in SDEA is proven. Furthermore, it is shown that positive b_{22} is necessary for two-port passivity and stiffness cannot be rendered if $I_m = 0$.

6.3 Performance Analysis

While the coupled stability of pHRI systems constitutes an imperative design criterion, the performance of the system is also significant for better behavior upon interactions. Thus, we determine the analytical equations for the evaluation of the system performance via transparency and Z_{width} concepts, as described in Section 3.3.

6.3.1 Transparency of the Two-Port Network

The two-port analysis enables investigation of the performance for all passive terminations through the use of the transparency concept. One can compare the h-matrix of the system to ideal transparency (given in Eqn. (3.3)) to assess the frequency-dependent characteristics of transparency. We have plotted each h-parameter for all frequencies in Section 6.4 in an attempt to observe the behavior. Furthermore, it is also possible to investigate it analytically at low and high frequencies.

Using the Eqn (6.4), the h-matrix converges to the following form at high frequencies.

$$\lim_{s \to \infty} \begin{bmatrix} F_{\text{int}} \\ v_e \end{bmatrix} = \begin{bmatrix} B_f & 0 \\ -1 & 1/b_{22} \end{bmatrix} \begin{bmatrix} -v_h \\ F_e \end{bmatrix}. \tag{6.18}$$

It is desirable to minimize B_f and maximize b_{22} to achieve better transparency at high frequencies. However, two-port passivity conditions impose an upper bound on b_{22} that depends on B_f which cannot be set to zero. Furthermore, ideal transparency is not achievable at high frequencies, as indicated by $h_{12} = 0$.

Note that transparency may not be crucial for frequencies that are over the force-control bandwidth of the system, while safety is a concern for these frequency ranges. This transparency analysis indicates that for a safe design, minimizing B_f

may help to decrease the magnitude of force transmitted to the operator at high frequencies. Note that if this is not feasible, the damper force may be mechanically limited, as proposed in [36].

At low frequencies, h-matrix of the system converge to ideal transparency as:

$$\lim_{s \to 0} \begin{bmatrix} F_{\text{int}} \\ v_e \end{bmatrix} = \begin{bmatrix} 0 & 1 \\ -1 & 0 \end{bmatrix} \begin{bmatrix} -v_h \\ F_e \end{bmatrix}. \tag{6.19}$$

Thanks to the integral gain I_f of the force controller, ideal transparency is achievable at low frequencies. As the frequency increases, the effect of I_f diminishes, and the proportional gain P_f prevails, as shown in Figure 6.5a. Also, virtual stiffness k_{22} dominates the virtual coupler behavior at low and medium frequencies.

6.3.2 Z-Width of the Two-Port Network

Passively achievable impedance range, Z_{width} , of the system, together with the minimum transmitted impedance, Z_{min} , are also investigated. The minimum impedance Z_{min} for SDEA under VSIC can be computed as

$$Z_{\min} = \frac{B_f M s^4 + [B_f (B + P_m) + K_f M] s^3 + [B_f I_m + K_f (B + P_m)] s^2 + K_f I_m s}{a_4 s^4 + a_3 s^3 + a_2 s^2 + a_1 s + a_0},$$
(6.20)

where $a_4 = M$ and $a_0 = K_f I_m I_f$. At low and high frequencies,

$$\lim_{s \to 0} Z_{\min} = 0 \tag{6.21}$$

$$\lim_{s \to \infty} Z_{\min} = B_f. \tag{6.22}$$

These limits recommend low physical damping, B_f , and high integral gain, I_f , of the force controller to achieve low Z_{\min} values.

The VC in Figure 6.3 does not affect the Z_{\min} of the system. However, if a parallel compliance G_{11} is employed, then this term increases the minimum impedance Z_{\min} .

Achievable impedance range Z_{width} for SDEA under VSIC can be computed as

$$Z_{\text{width}} = \frac{(b_{22}B_f P_m P_f)s^4 + \{b_{22}P_m P_f [B_f(\mu + \nu) + K_f] + k_{22}B_f P_m P_f\}s^3}{+\{k_{22}P_m P_f [B_f(\mu + \nu) + K_f] + b_{22}[K_f P_m P_f(\mu + \nu) + B_f I_m I_f]\}s^2}{+\{k_{22}[K_f P_m P_f(\mu + \nu) + B_f I_m I_f] + b_{22}K_f I_m I_f\}s + k_{22}K_f I_m I_f}},$$

$$= \frac{-(6.23)$$

where $a_4 = M$ and $a_0 = K_f I_m I_f$.

Evaluating Eqn. (6.23) at low and high frequencies,

$$\lim_{s \to 0} Z_{\text{width}} \to \infty \tag{6.24}$$

$$\lim_{s \to 0} s Z_{\text{width}} = k_{22} \tag{6.25}$$

$$\lim_{s \to \infty} Z_{\text{width}} = 0. \tag{6.26}$$

Eqn. (6.25) indicates that the stiffness transmitted to the operator is bounded at low frequencies by the stiffness of the VC. Consistent with the transparency analysis, these results indicate that SDEA cannot render impedances at high frequencies.

In conclusion, poor rendering performance is expected at high frequencies since SDEA assumes the dynamics of its physical filter for frequencies that are over the force control bandwidth of the device.

6.4 Numerical Evaluations

In this section, we investigate the effect of VC parameters on the two-port passivity, transparency, and transmitted impedance of the system. In particular, passivity bounds derived in Section 6.2 are studied through numerical simulations, considering the VC in Figure 6.3. VC parameters k_{22} and b_{22} are studied, systematically, to analyze their individual effects on the system behavior.

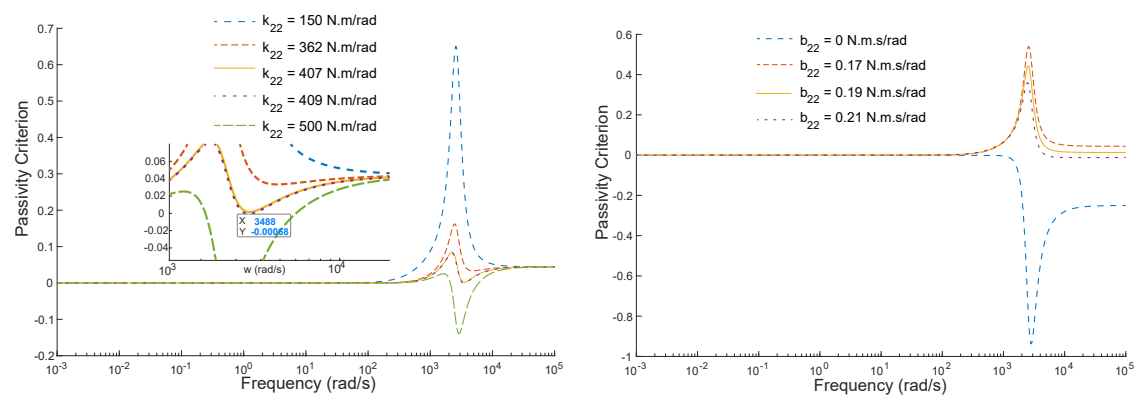
Table 6.1 presents the parameter values employed for the numerical simulations. The system parameters J, B, B_f , and K_f are determined by system identification. The control parameters P_m and P_f are selected based on the physical actuator limits, and the integral gains are tuned such that the system exhibits a decent tracking performance. We ensured that given these nominal parameters, the isolated system (i.e., h_{11}) is stable (according to Conditions (a)-(b) of Theorem 6.1), and positive real (according to Condition (c-i) of Theorem 6.1). In the next subsections, any improved parameter is selected within the constraints of Theorem 6.1.

Param. Description Nominal Value Unit K_f Stiffness of SDEA 362 N.m/rad B_f 0.05 Damping of SDEA N.m.s/rad JInertia of the actuator $6.399 \ 10^{-4}$ $kg.m^2$ BDamping of the actuator 0.169 N.m.s/rad P_m Proportional gain of the motion controller N.m.s/rad 0.28Integral gain of the motion controller 100 N.m/rad I_m P_f Proportional gain of the force controller 40 rad/N.m.s I_f Integral gain of the force controller 70 $rad/N.m.s^2$

Table 6.1: System parameters used for the numerical analysis

6.4.1 Passivity Analysis

Figure 6.4 presents the effect of VC stiffness, k_{22} , and damping, b_{22} , on the system performance. In these plots, passivity criterion corresponds to the evaluation of Condition (c-ii) of Theorem 3.2 (given as Eqn. (A.12) in the Appendix) according to the nominal values in Table 6.1. Since parameters in the table already satisfy



(a) Effect of VC stiffness, k_{22} , on two-port passivity

(b) Effect of VC damping, b_{22} , on two-port passivity

Figure 6.4: Numerical evaluations of Condition (c-ii) of Theorem 3.2

Conditions (a)–(c-i), each line in the plots must remain above zero for the two-port passivity.

Figure 6.4a reveals that a stiff virtual coupler adversely affects two-port passivity, causing the passivity criterion becomes negative. The upper bound on k_{22} , as derived in Section 6.2, can also be observed in this plot. For $k_{22} \gtrsim 408.5 \text{ N.m/rad}$, the system becomes two-port active. We also note that this value is greater than the physical stiffness of the SDEA in particular ($k_{22} \approx 1.17K_f$), which any known SEA cannot passively render (see Section 6.4.2 for a detailed discussion).

As presented in Section 6.2, VC damping b_{22} is bounded by $4B_f$. Figure 6.4b verifies that the absence or even slightly overuse of b_{22} makes the system two-port active.

Recall from Section 6.1.2 that k_{22} is a concave function of b_{22} when all other parameters are held constant (see Conditions (c-ii-1) and (c-ii-2) of Theorem 6.1). Therefore, it is possible to compute the b_{22} value that maximizes k_{22} for a given set of system parameters. Table 6.2 lists the results of several numeric optimizations conducted for achieving the maximum k_{22} .

In the analysis of the system, $(1-\alpha)$ regulates the state-dependent feed-forward term. Counter-intuitively, full cancellation of the physical interaction force adversely affects passivity, as observed in Table 6.2. Moreover, Conditions (c-ii-1) and (c-ii-2) of Theorem 6.1 include quadratic terms in α implying a concave behavior in α similar to the b_{22} case. Therefore, it is possible to maximize k_{22} by selecting both b_{22} and α optimally. For instance a partial cancellation with $\alpha = 0.9$, k_{22} can reach

Table 6.2: Maximum k_{22} values for the full-order (FO) system with different feedforward cancellation ratios compared to that of the FO system analyzed under absolute stability

	Optimal b_{22}	$\mathbf{Max} \ k_{22}$
System Configuration	[N.m.s/rad]	[N.m/rad]
With full feed-forward $(\alpha = 0)$	0.14	367.0
Without feed-forward ($\alpha = 1$)	0.17	408.5
With optimal feed-forward ($\alpha = 0.9$)	0.15	415.5
Without feed-forward (abs. stability)	0.13	432.0

a maximum stiffness of 415.5 N.m/rad.

For completeness, Table 6.2 provides the maximum achievable k_{22} value according to Condition (c-ii) of Theorem 2. Absolute stability analysis can relax the passivity bounds on k_{22} by 5% compared to the two-port passivity of the system without the feed-forward cancellation.

In summary, the maximum achievable k_{22} can be optimized via b_{22} and α , subject to the conditions of Theorem 6.1.

6.4.2 Performance Analysis

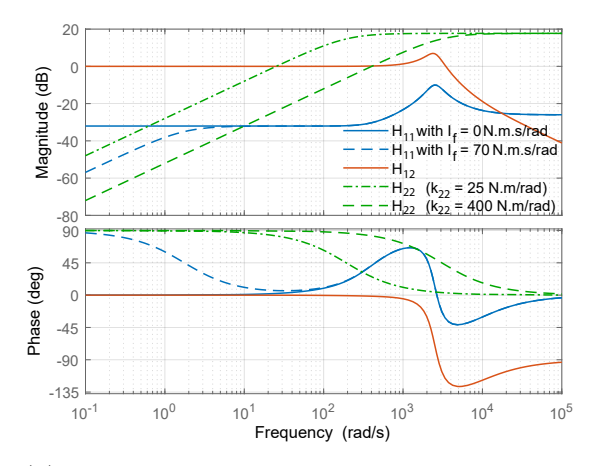
In Section 6.3.1, we have analytically studied the transparency of the system at the limit frequencies. To observe the system behavior at intermediate frequencies, Figure 6.5a plots the parameters of the h-matrix. Among these, h_{11} and h_{22} are the parasitic terms, and it can be observed that the transparency decreases as the frequency increases.

Increasing I_f and k_{22} improve the performance at low frequencies by decreasing parasitic effects due to h_{11} and h_{22} , respectively. However, I_f possesses an upper bound due to Condition (c-i) of Theorem 6.1. On the other hand, I_m slightly reduces the mid-frequency magnitudes of h_{11} while considerably enhancing k_{22}^{max} . In general, all proportional gains and damping terms (i.e., B_f and B) smooth out and push the peaks of the plots to higher frequencies. However, B_f dominates the high-frequency response, distorting the transparency.

On the other hand, α affects neither magnitude nor phase of h_{11} and h_{12} . However, the optimal selection of α increases the k_{22}^{max} , which improves the overall transparency of the system.

Null Impedance Rendering

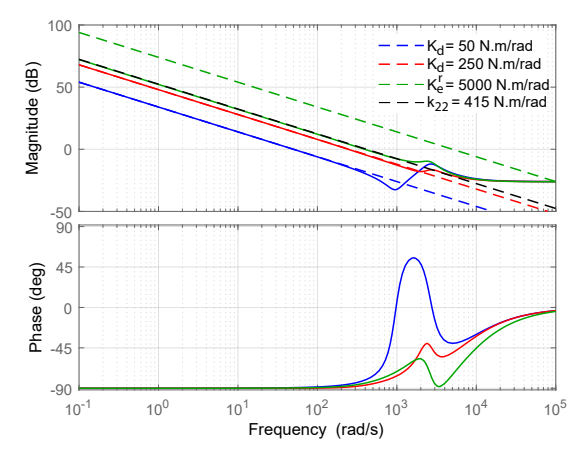
In this subsection, we study null impedance rendering, i.e., $Z_e = 0$. In this case, Z_{to} in Eqn. (3.4) reduces to h_{11} . Therefore, the following analysis appends to the comments on h_{11} in the transparency analysis.

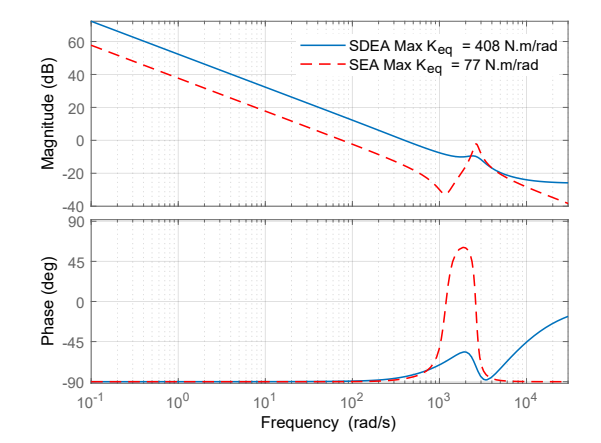


SDEA I_m= 301 N.m/rad
--SEA I_m= 213 N.m/rad
--SEA I_m= 213 N.m/rad
--SEA I_m= 213 N.m/rad
--SEA I_m= 213 N.m/rad
--SEA I_m= 213 N.m/rad
--SEA I_m= 213 N.m/rad
--SEA I_m= 213 N.m/rad
--SEA I_m= 213 N.m/rad
--SEA I_m= 213 N.m/rad
--SEA I_m= 213 N.m/rad
--SEA I_m= 213 N.m/rad
--SEA I_m= 213 N.m/rad
--SEA I_m= 213 N.m/rad
--SEA I_m= 213 N.m/rad
--SEA I_m= 213 N.m/rad
--SEA I_m= 213 N.m/rad
--SEA I_m= 213 N.m/rad
--SEA I_m= 213 N.m/rad
--SEA I_m= 213 N.m/rad
--SEA I_m= 213 N.m/rad
--SEA I_m= 213 N.m/rad
--SEA I_m= 213 N.m/rad
--SEA I_m= 213 N.m/rad
--SEA I_m= 213 N.m/rad
--SEA I_m= 213 N.m/rad
--SEA I_m= 213 N.m/rad
--SEA I_m= 213 N.m/rad

(a) The frequency response of the elements of the h-matrix to assess the transparency of the system. h_{11} and h_{22} are parasitic terms, and their magnitude plots are desired to be low. h_{12} should be 0 dB ($|h_{21}| = 0$ dB and not shown in this plot).

(b) Null impedance rendering of two-port passive SDEA compared to one-port passive SEA with maximum I_m values. SDEA increases the phase margin around the resonance frequency and allows higher controller gains.





(c) Pure spring rendering of the SDEA (solid lines) compared to the desired stiffness (dashed lines) for various virtual stiffness values.

(d) Pure stiffness rendering of two-port passive SDEA compared to one-port passive SEA. SDEA increases the maximum virtual stiffness that can be rendered.

Figure 6.5: Performance of the two-port passive SDEA under VSIC

Figure 6.5b compares the null impedance rendering performance of the investigated SDEA and the SEA in [59] under nominal system parameters. The phase plot of the figure exposes the improvement in the phase margin of the system due to the added parallel damping, which, in turn, grants increased bounds on the controller gains. In particular, higher I_m values can significantly improve the tracking

performance and disturbance rejection of the inner motion control loop, such that the inner motion controller can act as an ideal motion source within the control bandwidth. Furthermore, physical damping smooths the resonance peak that exists with SEA.

On the other hand, SDEA acts as a damper at high frequencies while SEA acts as a spring. For the safety of interaction, it may be necessary to mechanically limit the interaction forces while utilizing SDEA.

Spring Rendering

In this subsection, we study the case of pure spring rendering, i.e., $Z_e = K_e/s$. The impedance functions transmitted to the user under different virtual stiffness values are depicted in Figure 6.5c for the virtual coupler with $k_{22} = 415 \text{ N.m/rad}$ and $b_{22} = 0.15 \text{ N.m.s/rad}$.

Recall from Figure 6.3 that the virtual environment comprises the desired impedance and the VC. Therefore, for a virtual spring and an ideally transparent device, the operator would feel an equivalent spring of stiffness $K_{eq} = \frac{k_{22}K_e}{k_{22}+K_e}$. Then, it is possible to calculate the stiffness of the reference environment corresponding to the desired stiffness by solving the following equation for K_e .

$$K_e^r = \frac{k_{22}K_d}{k_{22} - K_d},\tag{6.27}$$

where K_e^r is the stiffness of the reference environment to render the desired stiffness, K_d . However, since the environment is passive, $K_d < k_{22}$, noting that:

$$\lim_{K_d \to k_{22}} K_e^r \to \infty. \tag{6.28}$$

Although two-port passivity allows all possible passive environments (even with unbounded parameters), Eqn. (6.27) reveals that the VC practically limits the rendering performance. Figure 6.5c verifies that, due to Eqn. (6.27), the SDEA can deliver the desired stiffness values below that of k_{22} and saturates at k_{22} for higher

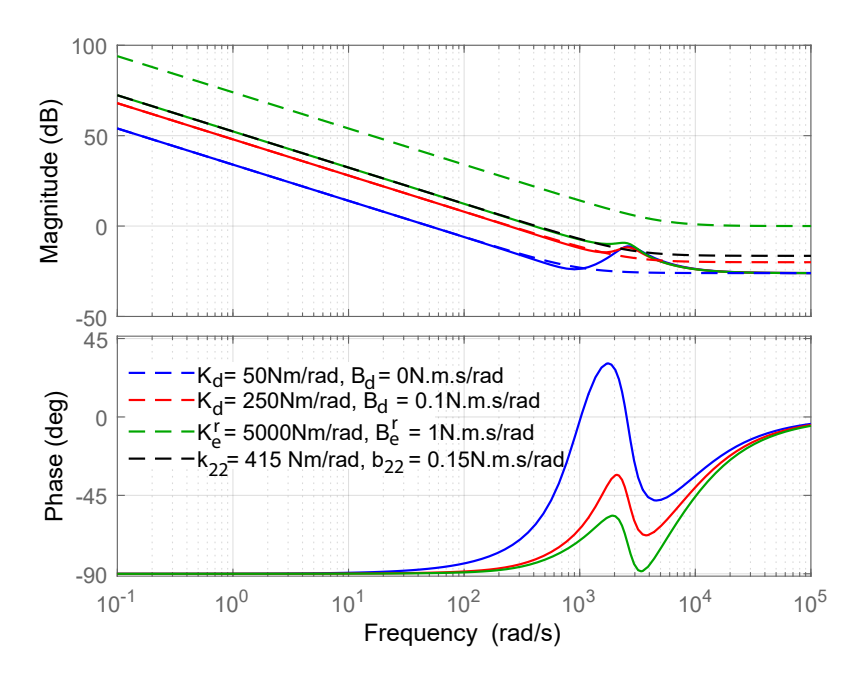


Figure 6.6: Kelvin-Voigt model rendering of the SDEA (solid lines) with the desired stiffness and damping values (dashed lines).

 K_e^r values (green dashed line in Figure 6.5c).

Figure 6.5d compares the performance of the SDEA with the SEA under identical system parameters. Thanks to the physical damper, SDEA can passively render a virtual spring five times stiffer than that of SEA can passively render.

Kelvin-Voigt Model Rendering

In this subsection, we study KV model rendering, i.e., $Z_e = K_e/s + B_e$. Figure 6.6 presents the KV model rendering performance of SDEA, given different environment parameter selections.

Note that the equivalent stiffness model introduced in the previous subsection is also valid in this model.

$$B_e^r = \frac{b_{22}B_d}{b_{22} - B_d},\tag{6.29}$$

where B_e^r is the reference environment damping to render the desired damping, B_d . As in the case of pure stiffness rendering, the maximum virtual damping is also limited by the damping of the VC. Similarly, the operator would feel the equivalent damping of the environment at high frequencies.

6.5 Discussion

In this section, we review the results of the two-port passivity of SDEA under VSIC with VC and present general design guidelines. We discuss the effects of the physical damping, virtual coupler, plant parameters, and controller gains in terms of the performance of haptic rendering within the two-port passivity limitations.

Independent of the application, it is generally a good practice to select high proportional gains that would not saturate the actuators within a reasonable range of frequencies [57], improving both stability and performance. The following remarks present the trade-offs in the design procedure.

6.5.1 The Necessity of Physical Damping

It has been well-established in the literature that SEA under VSIC cannot render the KV environment passively [57]. The inclusion of physical damping is crucial in that it enables SDEA to achieve KV model rendering while preserving one-port passivity. Remark 6.1 in Section 6.2 highlights that physical damping is also necessary to realize the two-port passivity of the device together with a VC.

The choice of the magnitude of B_f affects the high-frequency response, as presented in Figures 6.5b, 6.5d, and 6.6. In particular, the safety of interactions requires low B_f to limit the magnitude of impact forces. However, this also reduces the maximum b_{22} that the VC can employ, which limits the maximum k_{22} and the rendering performance. Therefore, one possible design strategy would be to select the maximum B_f that is acceptably safe for the application and iteratively trade-off the safety until the rendering performance becomes satisfactory.

6.5.2 The Necessity of Integral Gain of the Motion Controller

Section 6.2 proves that the integral gain I_m of the motion controller is necessary for the virtual coupler of SDEA under VSIC to have a non-zero stiffness. As discussed in Remark 6.3, this result is in good agreement with the one-port passivity analysis in [59] concluding that SEA cannot render a virtual spring when $I_m = 0$.

Note that the spring of the VC is not necessary for the passivity of the system while its magnitude sets an upper bound on the stiffness range that the device can display at low and intermediate frequencies. Moreover, the first term in Condition in (c-ii) of Theorem 6.1 implies that $I_f < I_m P_f/B$, requiring high values of I_m for high I_f .

6.5.3 The Effect of Virtual Coupler and System Dynamics on Two-Port Passivity and Transparency

We have shown in Section 6.2 that the damping b_{22} of the VC must be positive for the two-port passivity of the system and has an optimal value for maximizing the stiffness k_{22} of the VC, as captured by Conditions (c-ii) of Theorem 6.1. Such an optimization is valuable if the controller gains and system parameters do not display large changes.

Transparency and Z_{width} analyses indicate that k_{22} should be selected as stiff as possible, as the maximum achievable impedance transferred from the environment to the operator is dominantly limited by k_{22} . Especially, large K_f and I_m enhance k_{22}^{max} . Furthermore, null impedance rendering performance determines the minimum impedance Z_{min} of the system. In particular, increasing I_f and I_m improve Z_{min} at low and intermediate-frequencies, respectively, as shown in Figure 6.5a. However, increasing I_f decreases k_{22}^{max} .

As the state-dependent feed-forward compensation increases (i.e., as α decreases), the overall damping of the system deteriorates because α almost always acts as a

booster of b_{22} in Condition (c-ii) of Theorem 6.1. Therefore, the maximum value of k_{22} also decreases. In particular, VC stiffness, k_{22} , is a concave function of α when all other parameters are kept constant, as discussed in Section 6.4. As in the case of b_{22} , optimization of this parameter while keeping all other parameters constant may improve the rendering performance, as evidenced in Table 6.2.

6.6 Conclusion

We have provided the necessary and sufficient conditions for two-port passivity of SDEA under VSIC. Based on the newly established conditions, we have derived non-conservative passivity bounds for a virtual coupler. We have also proved the necessity of a physical damping term in parallel to the series elastic element to ensure two-port passivity (and absolute stability), even when a virtual coupler with a damping element is present. The physical damping element helps improve the control performance of the system, increasing the limits on the controller gains and the maximum stiffness of the virtual coupler. Furthermore, we have proved that, unlike SEA, SDEA can passively render virtual springs that are stiffer than the physical elastic element employed.

We have shown that feed-forward cancellation of the interaction force may deteriorate the upper limit on the stiffness of the virtual coupler.

Future works include an extension of these results to other control architectures and more general virtual coupler models.

Chapter 7

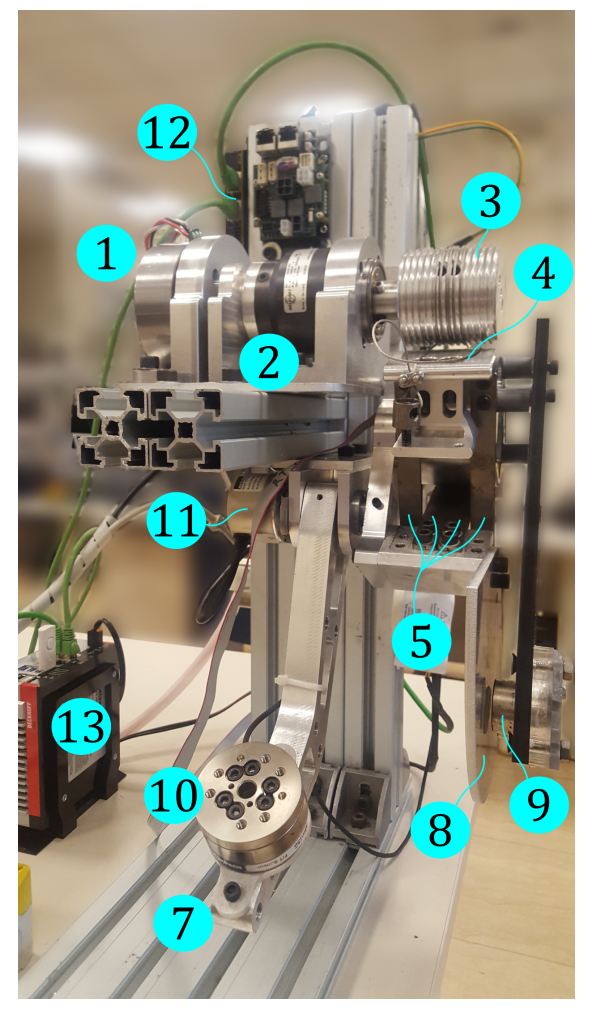
Experimental Evaluations

This chapter presents the experimental verification of the passivity bounds of SDEA under VSIC and a comparative study with SEA when convenient. The following section describes the physical setup and hardware properties. Since the analytic results derived in previous chapters require a good knowledge of the system, we first identify the physical properties of the setup, then provide an experimental procedure to validate the one-port and two-port passivity of the interaction system.

7.1 Experimental Setup

The test setup is designed [8] as a typical force-sensing SEA (the spring location is after the transmission, as categorized in [41]) and extended to an SDEA, as shown in Figure 7.1. A high-torque brushless DC motor (1) actuates the system through a series of transmission elements. The capstan drive (3, 4) allows passive back-drivability with minimum friction but requires more space for higher reduction. Inserting the low-reduction gearbox (2) preserves the back-drivability at an acceptable level and increases the torque capacity with a more compact design. Four cross-flexure leaf springs (5) connects the load-side capstan drum (4) and the end-effector (7). We implemented the Eddy-current method to create a contactless linear damping parallel to the spring. An aluminum plate (8) and magnet holder (9) are attached to

the end-effector (7) and the load-side drum (4), respectively, so that the relative motion between the plate and the magnets produces damping. In general, the user is expected to interact with the device through the end-effector. We also placed an extra F/T sensor (10) and a rotary encoder (11) on the end-effector to identify the spring rate and the damping ratio and validate the passivity of the interaction port.



3 8

components of the series damped elastic actuator used in the experiments

(a) The electromechanical and hardware (b) Removing the magnet plate (9) from the load-side drum (4), the system becomes a series elastic actuator.

Figure 7.1: Components of the experimental setup: Brushless DC motor (1), gearbox (2), motor-side capstan drum (3), load-side capstan drum (4), cross-flexure leaf springs (5), linear encoder measuring the spring deflection (6), end-effector (7), aluminum plate of eddy-current damper (8), permanent magnets and the holder plate (9), force/torque sensor for parameter estimation (10), rotary encoder measuring the end-effector angle for validations (11), motor driver (12), industrial PC (13).

The actuator is torque controlled using a high-speed MAXPOS Positioning Controller and can be commanded at a 10 kHz sampling rate. Therefore, all sensors read data at 10 kHz. The impedance, force, and velocity control loops run and update the actuator command 1 kHz unless specified otherwise. Due to the higher sensor rate, the noisy velocity measurements can be filtered with a high cutoff filter as investigated in [11]. Chawda, Celik, and O'Malley have reported in their study that the Z-width performance of a haptic device can peak using the finite difference method (FDM) cascaded with a seconder-order Butterworth filter with a cutoff frequency around 1.5 kHz. Therefore, we also filter all velocity signals in our controllers using FDM + filter at 1 kHz, which has performed decently compared to other sophisticated algorithms in [12].

7.1.1 System Identification

The passivity conditions presented in previous chapters require estimations of the reflected inertia and damping of the actuator and spring and damper of the physical filter. In series elastic actuation, it is possible to reduce the number of unknowns by isolating a component or a unit from the others without disassembling the system. However, we will present a procedure during the assembly. Therefore, the identification of the system in this work is twofold: parameter estimation of the actuation unit (i.e., the DC motor and the transmission elements) and that of the elastic coupling (i.e., the spring and eddy-current damping). Table 7.1 presents the results obtained in the following subsections.

Table 7.1: Estimated system parameters. All values are reflected to load-side.

Param.	Description	Estimated Value	Unit
K_f	Stiffness of SDEA	409	N.m/rad
B_f	Damping of SDEA	0.08	N.m.s/rad
J	Inertia of the actuator	0.8110	$\mathrm{kg.m}^2$
B	Damping of the actuator	1.2605	N.m.s/rad
r	Gear ratio	38.91	

Reflected Inertia and Damping of the Actuator

A common approach for the parameter identification of linear actuators is to measure the system response to sinusoidal inputs at the frequencies of interest [9] or a chirp signal swiping a frequency range continuously [59] and fit a transfer function model to the collected data given the number of poles and zeros. This procedure has become more convenient as third-party software is available with powerful preset algorithms.

If the workspace of the actuator is sufficiently large and the motor torque measurements are available, it is also possible to estimate the damping and inertia of the system separately. Knowing that the inertial effects diminish at constant velocities, the following relation holds.

$$B_i = \frac{T_i}{v_i} \tag{7.1}$$

where T_i is the actual motor torque and v_i is the actual motor velocity, both measured at the i^{th} sample time and B_i is the estimated motor damping at the same sample time. The motor target speed was set between 5-170 rad/s with 5 rad/s increments, covering the whole speed range of Maxon EC90. The procedure was conducted twice in the forward direction and twice in the backward direction. A Weibull function of form $B^{\text{fit}}(v) = abv^{(b-1)} \exp(-av^b)$ has been fit on each experiment (adjusted $R^2 \geq 0.9020$, RMSE ≤ 0.0013) using MATLAB Curve Fitting Toolbox, as shown in Figure 7.2. Although model parameters were slightly different in the forward and backward directions, we used the average of four experiments. In the passivity analysis, however, we selected the minimum damping value around the maximum velocity that our system can reach under load: $B_m = (8.3260)10^{-4} \text{ N.m.s/rad}$ at 150 rad/s. For varying damping, further underestimation can provide additional robustness against parameter uncertainties [46].

To estimate the inertia, we provided a ramp input and employed the following

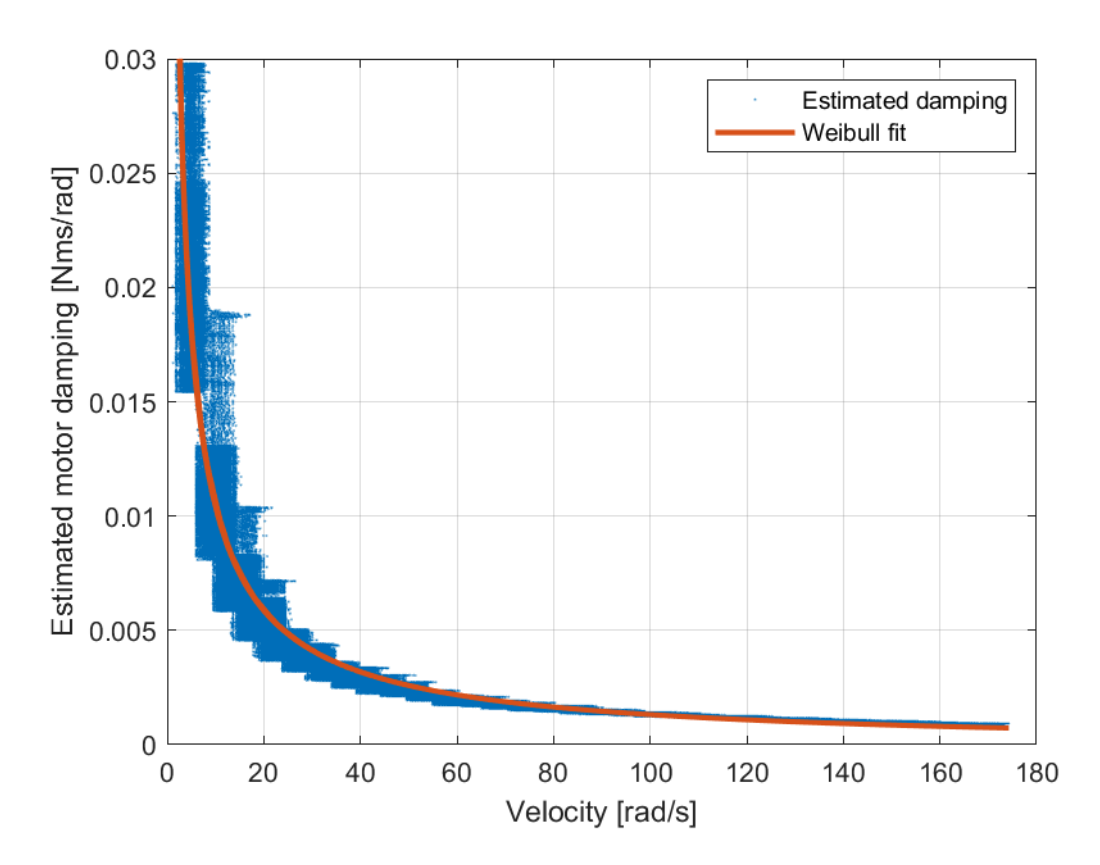


Figure 7.2: The cumulative damping in the actuator and the gearbox depends on the velocity. Among the curve models in MATLAB Curve Fitting Toolbox, Weibull model fits the best (Adjusted $R^2 = 0.9112$, RMSE = 0.0012).

relation using the Weibull function of the damping.

$$J_i = \frac{1}{a_i} \left(T_i - B^{\text{fit}}(v_i^a) v_i^a \right) \tag{7.2}$$

where T_i is the actual motor torque and v_i^a is the actual velocity filtered at 1 kHz in the new ramp experiments. $B_i^{\text{fit}}(v_i^a)$ is the estimated Weibull function and evaluated at the actual filtered velocity of the i^{th} sample time and a_i is the offline differentiation of the actual filtered velocity at the same sample time. The motor target speed was set between 0-170 rad/s increasing and decreasing at a constant rate of 2 and 4 rad/s². The procedure was conducted four times for each ramp input. A straight line of form $J^{\text{fit}}(t) = p_1 t + p_0$ has been fit on each experiment (adjusted $R^2 = 1$, RMSE ≤ 0.064) with bisquare weights for robustness against the noise and

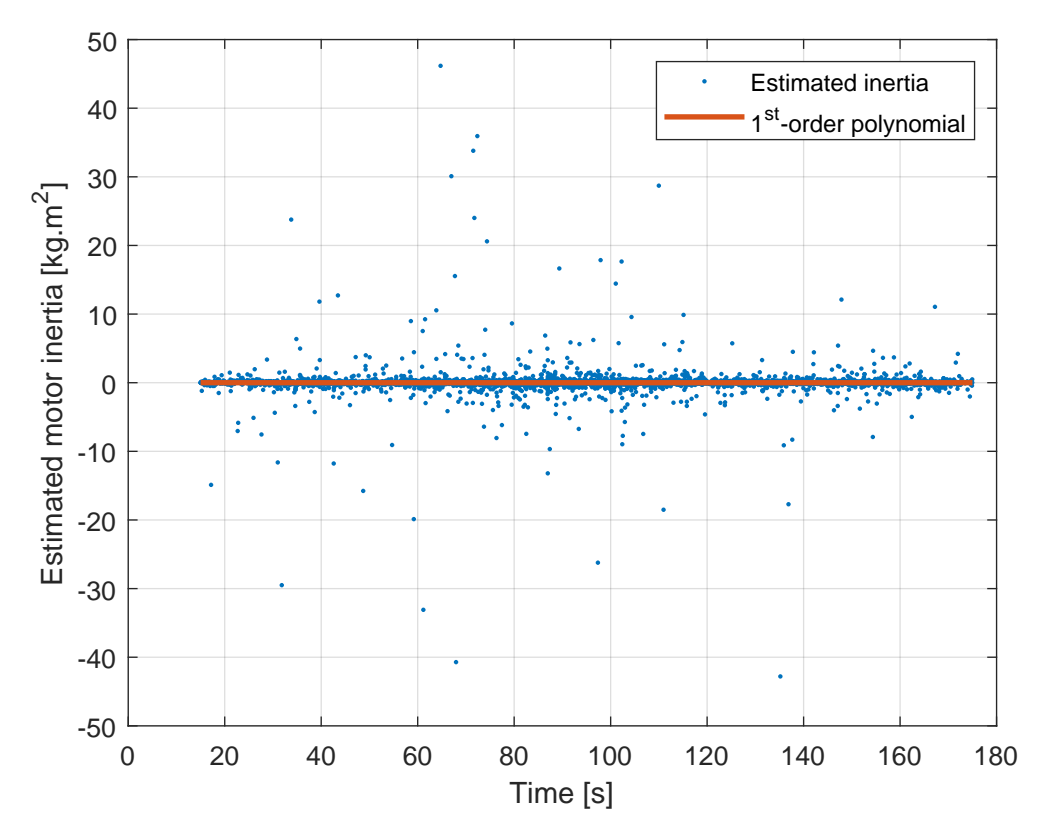


Figure 7.3: The cumulative inertia in the actuator and the gearbox is constant. The negative values were considered outliers. A first-order polynomial were used where the slope of the lines were always approximately zero (Adjusted $R^2 = 1$, RMSE = 0.0092).

outliers. Figure 7.3 shows one of the experimental data and the resulting fit. In all experiments, the parameter p_1 was at least three orders of magnitude less than p_0 such that the fit is almost constant, as expected. We used the average values of p_0 in all eight experiments as the estimated motor-side inertia: $J_m = (3.7498)10^{-4} \text{ kg.m}^2$, which is 72% of the expected inertia given the manufacturing and CAD data. Since overestimation of the inertia is suggested for robustness against parameter uncertainties [46], we used the manufacturing data as the motor-side reflected inertia: $J_m = (5.3569)10^{-4} \text{ kg.m}^2$.

Stiffness and Damping of the Physical Filter

Identification of the stiffness and damping is relatively more straightforward than that of actuator parameters. The stiffness is estimated by applying known forces at

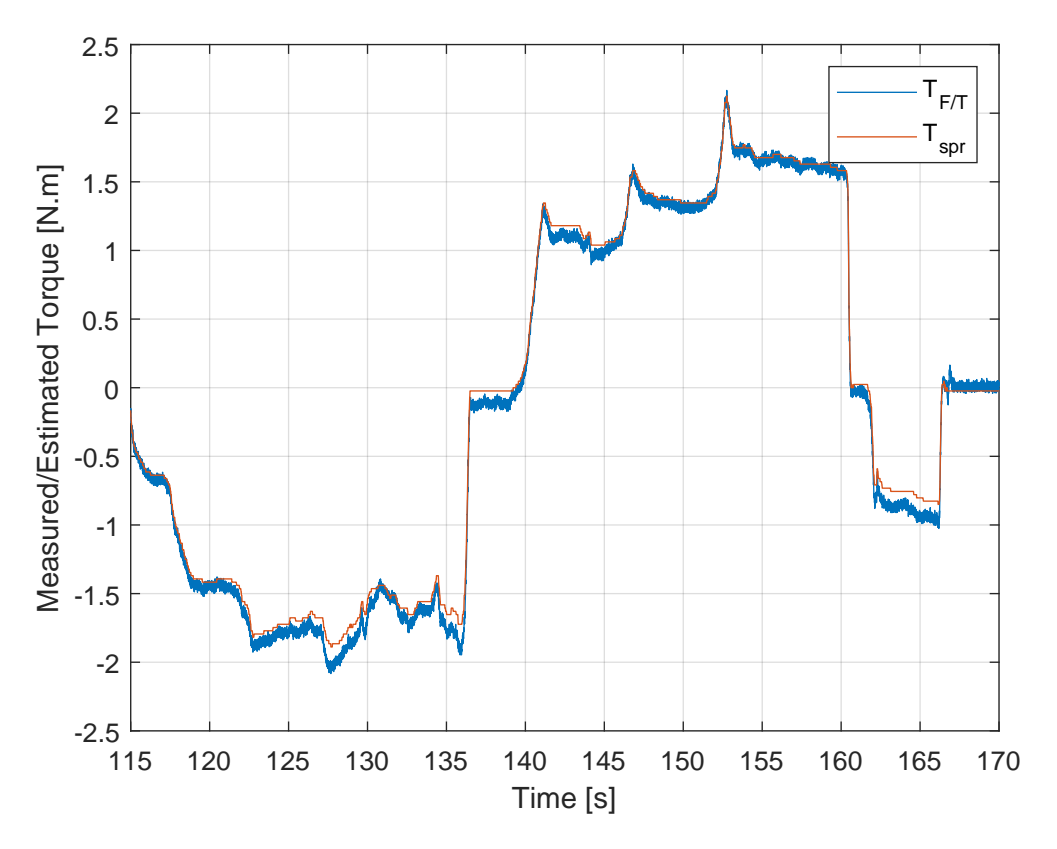


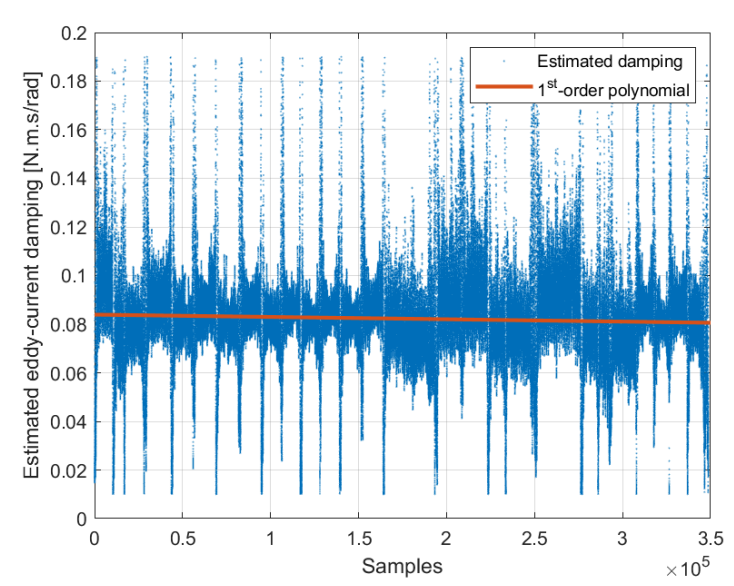
Figure 7.4: Validation of the torque estimation measuring the spring deflection.

the end-effector and measuring the deflection. We applied several constant forces on the force/torque sensor and estimated a joint torque constant of K = 409 N.m/rad. Figure 7.4 shows a validation data under slightly changing torque inputs.

The eddy-current damping depends on the distance between the aluminum plate and the magnets. Therefore, we prepared a test setup where the magnet plate is grounded at a chosen distance, as shown in Figure 7.5a. The aluminum plate is rotated by manually manipulating the end-effector, and its velocity is measured by the rotary encoder attached to the shaft of the end-effector, as shown by (11) in Figure 7.1. The force/torque sensor measures the reaction force due to the torque generated by the damping. Figure 7.5b shows the estimated damping for a distance of 15.3 mm between the plates (not from the aluminum plate to the magnets). The spikes in the figure correspond to the instants where the estimated velocity is close to zero, or other discretization effects prevail.

Table 7.2 lists all estimated values including the values corresponding to the





(a) Damping estimation (b) Damping values estimated at each sample for a plate dissetup tance of 15.3 mm (Adjusted $R^2 = 0.5139$, RMSE = 0.01315).

Figure 7.5: Estimation of the filter damping of SDEA. For this dataset, it is safer to underestimate the damping value as B = 0.08 N.m.s/rad.

other distances. Given these values, we select a plate distance of 15.3 mm and a damping value of 0.08 N.m.s/rad.

7.2 Verification of the Passivity Bounds

This section is not completed due to the pandemic conditions. However, the reader is referred to the online version of our studies [44], which will be updated upon completion of the experiments.

Table 7.2: Estimated damper values. The distances are measured between the two plates. Magnet tips are approximately 12.5 mm closer to the aluminum plate.

Distance [mm]	Value [N.m.s/rad]	Adj. R^2 value	RMSE
14.5	0.09859	0.3772	0.008559
$15.3 \; (Test \; 1)$	0.08493	0.3055	0.010640
15.3 (Test 2)	0.08681	0.4256	0.007813
16.1	0.07262	0.3625	0.010210

Chapter 8

Conclusion and Future Work

In this study, we have provided sufficient conditions for the one-port passivity of SDEA under VSIC while rendering the most commonly utilized linear virtual environment models. We discussed the effects of the physical damping, plant parameters, and controller gains within these passivity limitations on the performance of haptic rendering. We have also shown that the physical damping element helps improve the control performance of the system by adding phase lead that can be allocated to increase controller gains, resulting in more robust and responsive control.

We have also provided the necessary and sufficient conditions for the two-port passivity of SDEA under VSIC. Based on the newly established conditions, we have derived non-conservative passivity bounds for a virtual coupler. We have also proved the necessity of physical damping parallel to the series elastic element to ensure two-port passivity (and absolute stability), even when a virtual coupler with a damping element is present. The physical damping element helps improve the control performance of the system, increasing the limits on the controller gains and the maximum stiffness of the virtual coupler. Furthermore, we have proved that, unlike SEA, SDEA can passively render virtual springs stiffer than the physical elastic element employed. We have shown that feed-forward cancellation of the interaction force may deteriorate the upper limit on the stiffness of the virtual coupler.

The frequency-domain passivity analyses are highly valuable as they provide a

fundamental understanding of the underlying trade-offs governing the dynamics of the closed-loop system. For numerical implementations, less conservative paradigms, such as time-domain passivity [43], complementary stability [4,5], and mixed passivity and small-gain analyses [27] may be utilized to achieve better performance while still ensuring coupled stability of interaction.

Our ongoing works include investigating the effect of time delay and discretization on our passivity results. Future works include an extension of these results to other control architectures and more general virtual coupler models.

Appendix A

Proofs of the Two-Port Analysis

Proof of Lemma 6.2. If all the terms in any row of a Routh array are zero, then the characteristic equation has a pair of roots on the imaginary axis, and this special case may only occur at the odd-degree polynomial rows [48].

$$s^4$$
 a_4 a_2 a_0
 s^3 a_3 a_1
 s^2 $(a_2a_3 - a_1a_4)/a_3$ a_0
 s^1 $[a_1(a_2a_3 - a_1a_4) - a_0a_3^2]/(a_2a_3 - a_1a_4)$
 s^0 a_0

Since $a_i > 0$, the s^3 -row cannot become zero. The only possibility is to have $a_1(a_2a_3 - a_1a_4) - a_0a_3^2 = 0$ in the s^1 -row, which completes the proof.

Proof of Lemma 6.3. Since $a_1(a_2a_3-a_1a_4)=a_0a_3^2$, the impedance function Z(s) has a pair of poles as given by Lemma 6.2. Solving the auxiliary polynomial such that

$$f_a(s) = \frac{a_2 a_3 - a_1 a_4}{a_3} s^2 + a_0 = 0,$$

the roots are found to be at $s = \pm jp$ where

$$p = \sqrt{\frac{a_0 a_3}{a_2 a_3 - a_1 a_4}}.$$

For the residue, r, to be positive and real,

$$\operatorname{Im}(r) = 0: b_0 a_3^2 + b_4 a_1^2 - b_2 a_1 a_3 = \frac{a_1 a_3^2 (b_3 a_1 - b_1 a_3)}{a_2 a_3 - 2a_1 a_4}$$
(A.1)

$$\operatorname{Re}(r) > 0 : \frac{b_1 a_3 - b_3 a_1}{a_2 a_3 - 2a_1 a_4} > 0.$$
 (A.2)

We notice that Eqn. (A.2) appears at the right-hand side of Eqn. (A.1). Then, we can conclude the conditions given by Lemma 6.3.

Similar analysis shows the same results for s = -jp.

Proof of Lemma 6.4. Application of the Sturm's theorem results in the sign table below.

	N_0	N_1	N_2	N_3
x = 0	$sign(p_0)$	$sign(p_1)$	$sign(\sigma_3)$	$sign(\sigma_1)$
$x \to \infty$	$\operatorname{sign}(p_3)$	$sign(p_3)$	$sign(\sigma_2)$	$sign(\sigma_1)$

where

$$\sigma_1 = -4p_1\sigma_2^2 - 3p_3\sigma_3^2 + 4p_2\sigma_3\sigma_2$$

$$\sigma_2 = p_2^2 - 3p_3p_1$$

$$\sigma_3 = p_1p_2 - 9p_0p_3.$$

Non-negativeness of the polynomial p(x) allows roots of even multiplicity on the x-axis. However, proving positiveness of the polynomial provides the nonnegativeness at the limits of the derived conditions. Therefore, without loss of generality, the following proof ensures p(x) does not have real roots.

Non-negativeness of p(x) at the boundaries of $x \in [0, \infty)$ requires that $p_0 \ge 0$. Given $p_3 > 0$, all possible conditions that will result in an equal number of sign changes in the Sturm's sequence may be summarized as follows.

- (1) if $p_0 \ge 0$ and $\sigma_2 \le 0$ and $(\sigma_3 < 0 \lor \sigma_1 < 0)$,
- (2) if $p_0 \ge 0$ and $\sigma_2 > 0$ and one of the following holds
 - (i) $p_1 > 0 \land \sigma_3 > 0$,
 - (ii) $(p_1 > 0 \lor \sigma_3 < 0) \land \sigma_1 < 0.$

In Condition (1), rearranging $\sigma_2 \leq 0$ as $0 \leq p_2^2 \leq 3p_1p_3$ implies $p_1 \geq 0$ and $-\sqrt{3p_1p_3} \leq p_2 \leq \sqrt{3p_1p_3}$. To simplify the analysis, we can consider positive and negative cases of p_2 separately. If $p_2 \leq 0$ then $\sigma_3 = p_1p_2 - 9p_0p_3 < 0$, which is sufficient for Condition (1) to hold. On the other hand, if $p_2 > 0$ then we can rewrite $\sigma_1 < 0$ as $\sigma_3 > (4p_1\sigma_2^2 + 3p_3\sigma_3^2)/(4p_2\sigma_2)$. Note that, the right hand side of the inequality is always negative since $p_1 \geq 0$, $p_2 > 0$ and $\sigma_2 \leq 0$. Therefore, Condition (1) and positive realness are satisfied regardless of the signs of σ_1 and σ_3 if

$$-\sqrt{3p_1p_3} \le p_2 \le \sqrt{3p_1p_3}. (A.3)$$

In Condition (2), rearranging $\sigma_2 > 0$ as $p_2^2 > 3p_1p_3$ implies $p_2 < -\sqrt{3p_1p_3}$ or $p_2 > \sqrt{3p_1p_3}$ if $p_1 > 0$; otherwise, $p_2 \in \Re$.

Condition (2-i) requires $p_2 > 9p_0p_3/p_1$. However, Condition (2) and Eqn. (A.3) may be merged as follows

$$p_1 \ge 0 \land -\sqrt{3p_1p_3} \le p_2,$$

which is sufficient to satisfy the requirement in Condition (2-i). Condition (2-ii) is equal to $\sigma_3 < 0 \land \sigma_1 < 0$, since $p_1 > 0$ does not introduce any additional restriction. This completes the proof.

Proof of Theorem 6.1. Condition (a) of Theorem 3.2 requires the Routh-Hurwitz test on the diagonal elements of h-matrix. h_{22} is selected as passive; therefore, it is

stable. The characteristic equation of h_{11} is of the form considered in Lemma 6.1. Then, the system is stable if and only if the following condition holds.

$$0 < a_3 \left[K_f^2 P_m P_f(\mu + \nu) (\alpha + P_m P_f) + I_m (K_f \kappa_1 + B_f I_m I_f) \right]$$

+ $a_1 a_3 B_f P_m P_f(\mu + \nu) - a_1^2 M.$ (A.4)

In the case of Eqn. (A.4) is satisfied as equality, h_{11} has a pair of conjugate poles at the imaginary axis. For Condition (b), the following conditions ensure positive and real residues at those poles.

$$0 < \beta = [K_f(B + P_m) + B_f I_m][B + P_m + B_f(\alpha + P_m P_f)]$$

$$- B_f M[B_f I_m I_f + K_f P_m P_f(\mu + \nu)]$$
(A.5)

$$\{K_{f}I_{m}a_{3} - a_{1}[B_{f}(B + P_{m}) + K_{f}M]\}a_{3}^{2} = \beta\{a_{3}(I_{m} + K_{f}\alpha + P_{m}P_{f}[K_{f} + B_{f}(\mu + \nu)]) - 2M[B_{f}I_{m}I_{f} + K_{f}P_{m}P_{f}(\mu + \nu)]\}.$$
(A.6)

For Condition (c-i), positive realness of h_{22} is already assured by selection. On the other hand, $\text{Re}(h_{11})$ is reduced to the inequality below by Lemma 4.1, followed by the substitution of ω^2 by x.

$$0 \le B_f M^2 x^4 + B_f [B_f \kappa_3 + (B + P_m)^2 - 2I_m M] x^3$$
$$+ (K_f^2 \kappa_3 + B_f I_m^2 + B_f^2 I_m \kappa_1) x^2 + I_m K_f^2 \kappa_1 x, \tag{A.7}$$

where

$$\kappa_1 = P_f I_m - B I_f \tag{A.8}$$

$$\kappa_2 = B + P_m - M(\mu + \nu) \tag{A.9}$$

$$\kappa_3 = \alpha(B + P_m) + P_m P_f \kappa_2. \tag{A.10}$$

Eqn. (A.7) is of the form $r(x) = x (r_3 x^3 + r_2 x^2 + r_1 x + r_0)$ for $x \ge 0$. Then, Lemma 6.4 ensures $r(x) \ge 0$ for $x \ge 0$ providing the necessary and sufficient conditions for $r_3 x^3 + r_2 x^2 + r_1 x + r_0$. Lemma 6.4 requires that $r_0 \ge 0$, which implies

$$I_f \le \frac{I_m P_f}{B}.\tag{A.11}$$

Immediately following Lemma 6.4, we find the inequalities given in Condition (c-i) of Theorem 6.1.

Following the same steps as presented above, Condition (c-ii) leads to the polynomial below.

$$0 \leq \tau_1 b_{22} M^2 x^5 + (4b_{22} r_2 + b_{22}^2 \tau_2 - k_{22}^2 M^2) x^4$$

$$+ \left[4b_{22} r_1 + k_{22}^2 \tau_2 - b_{22}^2 (I_m + \alpha K_f)^2 \right] x^3 + \left[4b_{22} K_f^2 I_m \kappa_1 - k_{22}^2 (I_m + \alpha K_f)^2 \right] x^2,$$
(A.12)

where

$$\tau_1 = 4B_f - b_{22} \tag{A.13}$$

$$\tau_2 = 2M (I_m + \alpha K_f) - (B + P_m + \alpha B_f)^2.$$
 (A.14)

Eqn. (A.12) is of the form $t(x) = x^2(t_3x^3 + t_2x^2 + t_1x + t_0)$ for $x \ge 0$. Since Lemma 6.4 assumes $t_3 > 0$ and requires $t_0 \ge 0$ we have

$$0 < b_{22} \le 4B_f$$
 (A.15)

$$0 \le t_0 = 4b_{22}K_f^2 I_m \kappa_1 - k_{22}^2 (I_m + \alpha K_f)^2.$$
(A.16)

Although the condition $t_3 > 0$ allows negative b_{22} values, $t_0 \ge 0$ eliminates the non-positive region. Note that, in Eqn. (A.16), the first monomial should compensate for the negative effect of the second. Then, κ_1 must be greater than some positive constant, dictating more strict condition than Eqn. (A.11).

Immediately following the other conditions of Lemma 6.4, we find the	e inequalities
given in Condition (c-ii) of Theorem 6.1. This completes the proof.	

Bibliography

- [1] Richard J. Adams and Blake Hannaford. Stable haptic interaction with virtual environments. *IEEE Transactions on Robotics and Automation*, 15(3):465–474, 1999.
- [2] Alkiviadis G. Akritas and Panagiotis S. Vigklas. Counting the number of real roots in an interval with Vincent's theorem. *Bulletin Mathematique de la Societe des Sciences Mathematiques de Roumanie*, 53(3):201–211, 2010.
- [3] R. J. Anderson and M. W. Spong. Bilateral control of teleoperators with time delay. *IEEE Transactions on Automatic Control*, 34(5):494–501, 1989.
- [4] Y. Aydin, O. Tokatli, V. Patoglu, and C. Basdogan. Stable physical humanrobot interaction using fractional order admittance control. *IEEE Transactions* on *Haptics*, 11(3):464–475, 2018.
- [5] Yusuf Aydin, Ozan Tokatli, Volkan Patoglu, and Cagatay Basdogan. A computational multicriteria optimization approach to controller design for physical human-robot interaction. *IEEE Transactions on Robotics*, 36(6):1791–1804, 2020.
- [6] S. P. Buerger and N. Hogan. Complementary stability and loop shaping for improved human–robot interaction. *IEEE Transactions on Robotics*, 23(2):232– 244, 2007.
- [7] Andrea Calanca, Riccardo Muradore, and Paolo Fiorini. Impedance control of series elastic actuators: Passivity and acceleration-based control. *Mechatronics*, 47:37–48, 2017.
- [8] U. Caliskan, A. Apaydin, A. Otaran, and V. Patoglu. A series elastic brake pedal to preserve conventional pedal feel under regenerative braking. In IEEE/RSJ International Conference on Intelligent Robots and Systems, pages 1367–1373, 2018.
- [9] Umut Caliskan. A Series Elastic Brake Pedal for Improving Driving Performance under Regenerative Braking. M.sc. thesis, Sabanci University, 2020.

[10] Umut Caliskan and V. Patoglu. Efficacy of haptic pedal feel compensation on driving with regenerative braking. *IEEE Transactions on Haptics*, 13(1):175– 182, 2020.

- [11] Vinay Chawda, Ozkan Celik, and Marcia K. O'Malley. A Method for Selecting Velocity Filter Cut-Off Frequency for Maximizing Impedance Width Performance in Haptic Interfaces. *Journal of Dynamic Systems, Measurement, and Control*, 137(2):1–5, feb 2015.
- [12] Vinay Chawda, Ozkan Celik, and Marcia K. O'Malley. Evaluation of Velocity Estimation Methods Based on Their Effect on Haptic Device Performance. *IEEE/ASME Transactions on Mechatronics*, 23(2):604–613, 2018.
- [13] Michael Z.Q. Chen and Malcolm C. Smith. A note on tests for positive-real functions. *IEEE Transactions on Automatic Control*, 54(2):390–393, 2009.
- [14] Chee-Meng Chew, Geok-Soon Hong, and Wei Zhou. Series damper actuator: a novel force/torque control actuator. In *IEEE/RAS International Conference on Humanoid Robots*, volume 2, pages 533–546, 2004.
- [15] J. E. Colgate and N. Hogan. Robust control of dynamically interacting systems. *International Journal of Control*, 48(1):65–88, 1988.
- [16] J.E. Colgate. The Control of Dynamically Interacting Systems. Ph.d. dissertation, Massachusetts Institue of Technology, 1988.
- [17] J.E. Colgate and J.M. Brown. Factors affecting the Z-Width of a haptic display. In *IEEE International Conference on Robotics and Automation*, pages 3205–3210, 1994.
- [18] J.E. Colgate, M.C. Stanley, and J.M. Brown. Issues in the haptic display of tool use. In *IEEE/RSJ International Conference on Intelligent Robots and Systems. Human Robot Interaction and Cooperative Robots*, volume 3, pages 140–145, 1995.
- [19] José de Gea Fernández, Bingbin Yu, Vinzenz Bargsten, Michael Zipper, and Holger Sprengel. Design, modelling and control of novel series-elastic actuators for industrial robots. *Actuators*, 9(1):1–19, 2020.
- [20] Mark Dohring and Wyatt S. Newman. Admittance enhancement in force feedback of dynamic systems. In *IEEE International Conference on Robotics and Automation (ICRA)*, volume 1, pages 638–643, 2002.
- [21] Ahmetcan Erdogan, Besir Celebi, Aykut Cihan Satici, and Volkan Patoglu. AssistOn-Ankle: A reconfigurable ankle exoskeleton with series-elastic actuation. *Autonomous Robots*, pages 1–16, 2016.

[22] Ernest D Fasse. Stability robustness of impedance controlled manupulator coupled to passive environments. M.sc. thesis, Massachusetts Institute of Technology, 1987.

- [23] Michele Focchi, Gustavo A. Medrano-Cerda, Thiago Boaventura, Marco Frigerio, Claudio Semini, Jonas Buchli, and Darwin G. Caldwell. Robot impedance control and passivity analysis with inner torque and velocity feedback loops. Control Theory and Technology, 14(2):97–112, 2016.
- [24] E. Garcia, J.C. Arevalo, G. Muñoz, and P. Gonzalez-de Santos. Combining series elastic actuation and magneto-rheological damping for the control of agile locomotion. *Robotics and Autonomous Systems*, 59(10):827–839, 2011.
- [25] Paul G. Griffiths, R. Brent Gillespie, and Jim S. Freudenberg. Performance/Stability Robustness Tradeoffs Induced by the Two-Port Virtual Coupler. In *IEEE Symposium on Haptic Interfaces for Virtual Environment and Teleoperator Systems*, pages 193–200, 2006.
- [26] A. Haddadi and K. Hashtrudi-Zaad. Bounded-impedance absolute stability of bilateral teleoperation control systems. *IEEE Transactions on Haptics*, 3(1):15–27, 2010.
- [27] Kevin Haninger and Masayoshi Tomizuka. Robust passivity and passivity relaxation for impedance control of flexible-joint robots with inner-loop torque control. *IEEE/ASME Transactions on Mechatronics*, 23(6):2671–2680, 2018.
- [28] B. Hannaford and Jee-Hwan Ryu. Time-domain passivity control of haptic interfaces. *IEEE Transactions on Robotics and Automation*, 18(1):1–10, 2002.
- [29] Blake Hannaford. A design framework for teleoperators with kinesthetic feedback. *IEEE Transactions on Robotics and Automation*, 5(4):426–434, 1989.
- [30] Keyvan Hashtrudi-Zaad and Septimiu E. Salcudean. Analysis of Control Architectures for Teleoperation Systems with Impedance/Admittance Master and Slave Manipulators. *The International Journal of Robotics Research*, 20(6):419–445, 2001.
- [31] Simon Haykin. *Active network theory*. Reading, Mass. : Addison-Wesley Pub. Co, 1970.
- [32] Russell D Howard. Joint and actuator design for enhanced stability in robotic force control. Phd thesis, Massachusetts Institute of Technology, 1990.
- [33] Jonathan Hurst, Alfred Rizzi, and Daan Hobbelen. Series elastic actuation: Potential and pitfalls. In *International conference on climbing and walking robots*, 2004.

[34] A. Kamadan, G. Kiziltas, and V. Patoglu. Co-design strategies for optimal variable stiffness actuation. *IEEE/ASME Transactions on Mechatronics*, 22(6):2768–2779, 2017.

- [35] A. Kamadan, G. Kiziltas, and V. Patoglu. A systematic design selection methodology for system-optimal compliant actuation. *Robotica*, pages 1–19, 2018.
- [36] Min Jun Kim, Alexander Werner, Florian Christoph Loeffl, and Christian Ott. Enhancing joint torque control of series elastic actuators with physical damping. In *IEEE International Conference on Robotics and Automation (ICRA)*, pages 1227–1234, 2017.
- [37] Kyoungchul Kong, Joonbum Bae, and M. Tomizuka. A compact rotary series elastic actuator for human assistive systems. *IEEE/ASME Transactions on Mechatronics*, 17(2):288–297, 2012.
- [38] Matteo Laffranchi, Lisha Chen, Navvab Kashiri, Jinoh Lee, Nikos G. Tsagarakis, and Darwin G. Caldwell. Development and control of a series elastic actuator equipped with a semi active friction damper for human friendly robots. *Robotics and Autonomous Systems*, 62(12):1827–1836, 2014.
- [39] Matteo Laffranchi, Nikos G. Tsagarakis, and Darwin G. Caldwell. A compact compliant actuator (CompAct) with variable physical damping. In *IEEE International Conference on Robotics and Automation*, pages 4644–4650, 2011.
- [40] Dale A. Lawrence. Stability and transparency in bilateral teleoperation. *IEEE Transactions on Robotics and Automation*, 9(5):624–637, 1993.
- [41] Chan Lee, Suhui Kwak, Jihoo Kwak, and Sehoon Oh. Generalization of Series Elastic Actuator Configurations and Dynamic Behavior Comparison. *Actuators*, 6(3):26, aug 2017.
- [42] H. Lee, J. Lee, J. Ryu, and S. Oh. Relaxing the conservatism of passivity condition for impedance controlled series elastic actuators. In *IEEE/RSJ International Conference on Intelligent Robots and Systems*, pages 7610–7615, 2019.
- [43] Hyunwook Lee, Jee-Hwan Ryu, Jinoh Lee, and Sehoon Oh. Passivity controller based on load-side damping assignment for high stiffness controlled series elastic actuators. *IEEE Transactions on Industrial Electronics*, 68(1):871–881, 2021.
- [44] Ugur Mengilli, Umut Caliskan, Zeynep Ozge Orhan, and Volkan Patoglu. Two-port analysis of stability and transparency in series damped elastic actuation. CoRR, 2020.

[45] H. Munawar and V. Patoglu. Gravity-Assist: A series elastic body weight support system with inertia compensation. In *IEEE/RSJ International Conference on Intelligent Robots and Systems*, pages 3036–3041, 2016.

- [46] Wyatt S. Newman. Stability and performance limits of interaction controllers. Journal of Dynamic Systems, Measurement, and Control, 114(4):563–570, 1992.
- [47] Jakob Oblak and Zlatko Matjačić. Design of a series visco-elastic actuator for multi-purpose rehabilitation haptic device. *Journal of NeuroEngineering and Rehabilitation*, 8(1):3, 2011.
- [48] K Ogata. *Modern Control Engineering*. Prentice Hall, Upper Saddle River, 5th edition, 2009.
- [49] G.A. Pratt, P. Willisson, C. Bolton, and A. Hofman. Late motor processing in low-impedance robots: impedance control of series-elastic actuators. *American Control Conference*, pages 3245–3251, 2004.
- [50] Gill A. Pratt and Matthew M. Williamson. Series elastic actuators. In IEEE/RSJ International Conference on Intelligent Robots and Systems. Human Robot Interaction and Cooperative Robots, volume 1, pages 399–406, 1995.
- [51] David W. Robinson, Jerry E. Pratt, D.J. Paluska, and Gill A. Pratt. Series elastic actuator development for a biomimetic walking robot. In *IEEE/ASME International Conference on Advanced Intelligent Mechatronics (AIM)*, volume 39, pages 561–568, 1999.
- [52] Jee-Hwan Ryu, Dong-Soo Kwon, and B. Hannaford. Stability guaranteed control: time domain passivity approach. *IEEE Transactions on Control Systems Technology*, 12(6):860–868, 2004.
- [53] Mine Sarac, Mehmet Alper Ergin, Ahmetcan Erdogan, and Volkan Patoglu. AssistOn-Mobile: A series elastic holonomic mobile platform for upper extremity rehabilitation. *Robotica*, 32:1433–1459, 2014.
- [54] Jonathon Sensinger and Richard Weir. Improvements to series elastic actuators. In *IEEE/ASME International Conference on Mechatronics and Embedded Systems and Applications*, pages 1–7, 2006.
- [55] Jonathon Sensinger and Richard F. Weir. Unconstrained impedance control using a compact series elastic actuator. In *IEEE/ASME International Conference on Mechatronics and Embedded Systems and Applications*, pages 1–6, 2006.
- [56] Yusuf Mert Senturk and Volkan Patoglu. MRI-VisAct: A bowden cable-driven mri compatible series viscoelastic actuator. *Transactions of the Institute of Measurement and Control, Sage*, 40(8):2440–2453, 2018.

[57] Nevio Luigi Tagliamonte and Dino Accoto. Passivity constraints for the impedance control of series elastic actuators. *Institution of Mechanical Engineers, Part I: Journal of Systems and Control Engineering*, 228(3):138–153, 2014.

- [58] Lawrence J Tognetti. Improved design and performance of haptic two-port networks through force feedback and passive actuators. Ph.d. thesis, Georgia Institute of Technology, 2005.
- [59] Fatih Emre Tosun and Volkan Patoglu. Necessary and sufficient conditions for the passivity of impedance rendering with velocity-sourced series elastic actuation. *IEEE Transactions on Robotics*, 36(3):757–772, 2020.
- [60] Heike Vallery, Ralf Ekkelenkamp, Herman van der Kooij, and Martin Buss. Passive and accurate torque control of series elastic actuators. In *IEEE/RSJ International Conference on Intelligent Robots and Systems*, pages 3534–3538, 2007.
- [61] Heike Vallery, Jan Veneman, Edwin H.F. van Asseldonk, Ralf Ekkelenkamp, Martin Buss, and Herman van der Kooij. Compliant actuation of rehabilitation robots. *IEEE Robotics & Automation Magazine*, 15(3):60–69, 2008.
- [62] J. F. Veneman, R. Ekkelenkamp, R. Kruidhof, F. C. T. van der Helm, and H. van der Kooij. A series elastic- and bowden-cable-based actuation system for use as torque actuator in exoskeleton-type robots. *The International Journal of Robotics Research*, 25(3):261–281, 2006.
- [63] B. Willaert, M. Franken, H. Van Brussel, and E.B. Vander Poorten. On the use of shunt impedances versus bounded environment passivity for teleoperation systems. In *IEEE International Conference on Robotics and Automation* (ICRA), pages 2111–2117, 2011.
- [64] Gordon Wyeth. Demonstrating the safety and performance of a velocity sourced series elastic actuator. In *IEEE International Conference on Robotics and Automation (ICRA)*, pages 3642–3647, 2008.
- [65] Michael Zinn, Oussama Khatib, Bernard Roth, and J. Kenneth Salisbury. Large workspace haptic devices - a new actuation approach. In Symposium on Haptic Interfaces for Virtual Environment and Teleoperator Systems, pages 185–192, 2008.